

# Photolysis of Atmospheric Ozone in the Ultraviolet Region

Yutaka Matsumi\*

*Solar Terrestrial Environment Laboratory and Graduate School of Science, Nagoya University, Toyokawa 442-8505, Japan*

Masahiro Kawasaki

*Department of Molecular Engineering and Graduate School of Global Environmental Studies, Kyoto University, Kyoto 606-8501, Japan*

*Received February 18, 2003*

## Contents

1. Introduction	4767
2. Absorption Spectrum and Its Assignment	4769
3. O( <sup>1</sup> D) Formation from the Photolysis of Ozone	4770
3.1. O( <sup>1</sup> D) Formation in the Atmosphere	4770
3.2. O( <sup>1</sup> D) Quantum Yield Measurements	4770
3.3. Experimental Techniques for O( <sup>1</sup> D) Yield Measurements	4771
3.4. Absolute Values of the O( <sup>1</sup> D) Quantum Yield	4772
3.5. O( <sup>1</sup> D) Quantum Yield between 306 and 328 nm	4773
3.6. O( <sup>1</sup> D) Quantum Yield below 306 nm and above 328 nm	4774
3.7. Physical Processes of O( <sup>1</sup> D) Formation	4775
3.7.1. Photodissociation of Vibrationally Excited Ozone	4775
3.7.2. Spin-Forbidden Processes	4776
4. Implications for Atmospheric Chemistry	4776
4.1. Formation O <sub>2</sub> (v) in the Photolysis of Ozone and Subsequent Reactions	4776
4.2. O <sub>2</sub> (A <sup>1</sup> Δ <sub>g</sub> ) and O <sub>2</sub> (b <sup>1</sup> Σ <sup>+</sup> <sub>g</sub> ) Detection from the Photolysis of Ozone	4777
4.3. Nonlocal Thermal Equilibrium (non-LTE) Translational Distribution Produced by UV Photolysis of Ozone	4778
4.4. N <sub>2</sub> O Formation Associated with UV Photodissociation of Ozone	4779
5. Conclusions	4779
6. Acknowledgments	4779
7. References	4779



Yutaka Matsumi earned his doctorate degree in Chemistry at Tokyo Institute of Technology in 1981. After he spent several years in private companies, he was an associate professor at Hokkaido University for nine years. He has been at the Solar-Terrestrial Environment Laboratory at Nagoya University since 1997. His research interests include chemical reaction processes in the atmosphere and development of instruments for atmospheric gases and particles.



Masahiro Kawasaki received his doctorate degree from the Chemistry Department of Tokyo Institute of Technology under the supervision of Professor Ikuzo Tanaka and was a postdoctoral fellow of Professor Richard Bersohn's laboratory at Columbia University. He was a professor in Hokkaido University for 10 years and now has been at Kyoto University for 6 years. His research interests are photodissociation dynamics, elementary reactions, and atmospheric radical reactions.

## 1. Introduction

The near-ultraviolet (UV) photochemistry of ozone remains a topic of great contemporary interest. Figure 1 shows the absorption spectrum of ozone in the UV region between 195 and 345 nm at 295 K, which is plotted using the data measured by Malicet et al.<sup>1</sup> The UV absorption spectrum of O<sub>3</sub> consists of two bands. The wide bell-shaped absorption peaking at approximately 250 nm is called the Hartley band.

The vibrational structure in the long wavelength edge of Hartley band in the 310–360 nm region is called the Huggins band. Table 1 lists the threshold wavelengths for the dissociation processes to various

\* To whom correspondence should be addressed. Fax: +81-533-89-5593. E-mail: matsumi@stelab.nagoya-u.ac.jp.

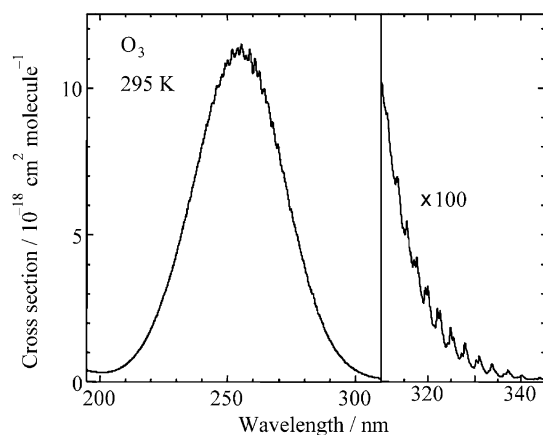
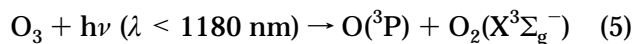
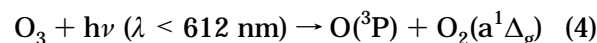
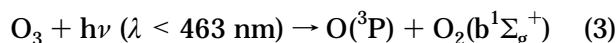
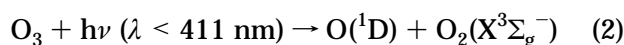
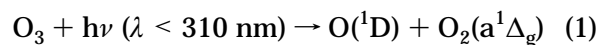


**Figure 1.** Absorption spectrum of ozone in the ultraviolet region. The cross sections are taken from the data presented by Malicet et al.<sup>1</sup>

**Table 1. Energetically Possible Combinations of O Atom and O<sub>2</sub> Molecule in the Photolysis of Ozone with Their Threshold Wavelengths (in nm)<sup>2</sup>**

O/O <sub>2</sub>	X <sup>3</sup> Σ <sup>-</sup> <sub>g</sub>	a <sup>1</sup> Δ <sub>g</sub>	b <sup>1</sup> Σ <sup>+</sup> <sub>g</sub>	A <sup>3</sup> Σ <sup>+</sup> <sub>u</sub>	B <sup>3</sup> Σ <sup>-</sup> <sub>u</sub>
<sup>3</sup> P	1180	611	463	230	173
<sup>1</sup> D	411	310	266	168	136
<sup>1</sup> S	237	200	180	129	109

electronic states of O and O<sub>2</sub> in the photolysis of ozone.<sup>2</sup> Figure 2 shows the solar actinic flux at 0, 20, and 40 km altitude calculated for a solar zenith angle of 50° using a program presented by Kylling et al.<sup>3</sup> The solar spectra indicate that the following photodissociation processes are important in the troposphere and stratosphere



where the wavelengths given in parentheses indicate the thermodynamic thresholds for the fragmentations which are listed in Table 1. From the viewpoint of atmospheric chemistry, the O(<sup>1</sup>D) atom is the most important product of ozone photolysis. Ozone photolysis is the source of the O(<sup>1</sup>D) atoms in the lower atmosphere. Here, we call the probability of the formation of an O(<sup>1</sup>D) atom in the photolysis of a single ozone molecule at a given photolysis wavelength the "O(<sup>1</sup>D) quantum yield". The O(<sup>3</sup>P) atoms produced from the O<sub>3</sub> photolysis have no atmospheric chemical relevance since they recombine immediately with O<sub>2</sub> in a termolecular reaction and reform ozone.

Most of the O(<sup>1</sup>D) atoms produced from the photolysis of ozone in the atmosphere are efficiently de-excited to ground-state oxygen atoms, O(<sup>3</sup>P), by collisions with N<sub>2</sub> molecules which are the main constituent of the air, although the radiative lifetime of O(<sup>1</sup>D) to the lower state, O(<sup>3</sup>P), is very long (ca.

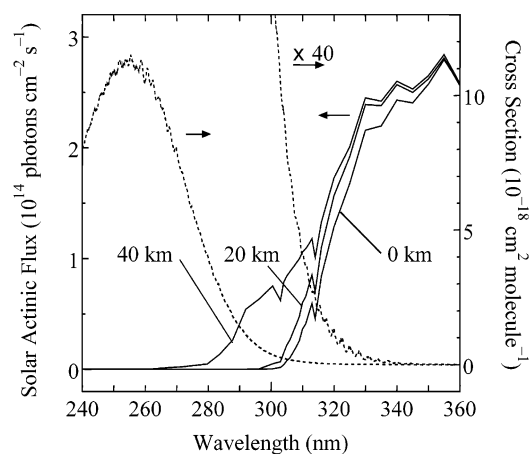


**Figure 2.** Solar actinic flux spectra in the ultraviolet wavelength region at altitudes of 0, 20, and 40 km which are calculated with the solar zenith angle of 50°, no cloud, and the surface albedo of 0.3 using a program presented by Kylling et al.<sup>3</sup> The dotted curve indicates the absorption cross-section spectrum of ozone.

148 s). Therefore, the concentration of O(<sup>1</sup>D) in the atmosphere is very small. The primary reason for the extreme importance of this very low abundance species is that a small fraction of O(<sup>1</sup>D) reactions create highly reactive species from highly unreactive species; these minor pathways for O(<sup>1</sup>D) loss are often the major pathway for the generation of the reactive species. OH radicals in the stratosphere and troposphere and NO (and consequently NO<sub>2</sub>) in the stratosphere are produced from reaction of O(<sup>1</sup>D) with H<sub>2</sub>O and N<sub>2</sub>O.



The reactive species created by these reactions, OH and NO, are immensely important in atmospheric chemistry. OH radicals initiate the atmospheric degradation of most natural and anthropogenic emissions entering the atmosphere. OH reactions provide pathways that convert species that are active in ozone destruction chemistry to species which are inactive, and at other times OH radicals convert inactive into active species. OH is a major catalyst for lower stratospheric ozone removal. Nitric oxide is a crucial ingredient of the stratosphere. Reaction 2 leads to NO<sub>x</sub> (NO + NO<sub>2</sub>), which is the most important catalyst for ozone destruction in most of the stratosphere. NO<sub>x</sub> also suppresses the catalytic destruction of ozone by halogens by sequestering them in unreactive forms such as ClONO<sub>2</sub>. Therefore, the quantum yield for O(<sup>1</sup>D) production in the UV photolysis of ozone (O<sub>3</sub>) is a key input for modeling calculations in the atmospheric chemistry.

In this paper, we review the published studies concerning the UV photodissociation of ozone of relevance to stratospheric and tropospheric chemistry. The formation of O(<sup>1</sup>D) is the most important aspect of the ozone photolysis. The contents are (1) the ultraviolet absorption spectrum of ozone and its assignments, (2) the determination of the O(<sup>1</sup>D)

quantum yield in the photolysis of ozone in the UV region, and (3) the temperature and photolysis wavelength dependence of the O(<sup>1</sup>D) quantum yields. Then, we review some topics of the studies on the atmospheric roles of the ozone photodissociation, such as the vibrationally or translationally hot fragments produced from the photolysis of ozone molecules in the UV region.

The UV photochemistry of ozone has been the subject of previous reviews by Schiff,<sup>4</sup> Wayne,<sup>5</sup> and Steinfeld et al.<sup>6</sup> Absorption cross sections and photodissociation processes of ozone have been evaluated, and recommended data have been published in the comprehensive assessments of kinetic and photochemical data for atmospheric chemistry by the IUPAC subcommittee<sup>7,8</sup> and in the chemical kinetics and photochemical data books for use in stratospheric modeling by the NASA Jet Propulsion Laboratory (NASA/JPL).<sup>9–12</sup>

## 2. Absorption Spectrum and Its Assignment

The ozone molecule has strong absorption in the UV region, which protects life on earth from the harmful UV sunlight in the stratosphere.<sup>13</sup> The UV absorption spectrum consists of a strong continuum (Hartley band) with a maximum near 250 nm which is overlapped in the longer wavelength region (>310 nm) by diffuse vibrational structures corresponding to the Huggins band (see Figure 1). The Huggins and Hartley band cross sections are very important for atmospheric modeling. In the Hartley band the temperature effect is found to be weak. At the mercury line wavelength ( $\lambda = 253.65$  nm), near the maximum of the absorption, the cross section increases by about 1% when the temperature decreases from 295 to 218 K.<sup>14,15</sup> On the other hand, in the Huggins band, which has steep shape structure, there is a strong variation of the values with temperature, particularly in the regions of low absorption between the peaks. An early review on the ozone UV absorption was presented in a WMO report<sup>16</sup> in 1986. Yoshino et al.<sup>17</sup> measured the cross sections at temperatures 195, 228, and 295 K at 12 wavelengths between 185 and 254 nm using various atomic line sources. Molina and Molina<sup>18</sup> reported the absolute cross sections of ozone at 226, 263, and 298 K in the 185- to 350-nm wavelength range at intervals of 0.5 nm using a double-beam spectrophotometer with a resolution of 0.07 nm. Voigt et al.<sup>19</sup> measured the absolute cross sections in the wavelength region 230–850 nm at temperature 203–293 K using a Fourier transform spectrometer at a spectral resolution of 5.0 cm<sup>-1</sup>. Brion, Malicet, and co-workers<sup>1,14</sup> obtained the high-resolution absorption cross sections of ozone at 218, 228, 243, 273, and 295 K in the range 195–345 nm (in air wavelength) in steps of 0.01 nm using a 0.64-m monochromator and a deuterium or tungsten lamp with the spectral line width of 0.01–0.02 nm. The differences between the absolute cross sections presented by Molina and Molina<sup>18</sup> and Brion et al.<sup>14</sup> are within 2–3% at room temperature. Malicet et al.<sup>1</sup> compared the sets of the absolute values obtained by them and those by Yoshino et al.<sup>17</sup> at 228 K at 13 fixed wavelengths covering the spectral range 230–

345 nm and found that the values agreed to within 3%. The comparison between the absolute cross sections obtained by Malicet et al.<sup>1</sup> at 228 K and those by Molina and Molina<sup>18</sup> at 226 K indicated that the differences were less than 1% below 240 nm and within 3% for greater wavelengths. Recently, a review of the absorption cross sections of ozone has been published by Orphal.<sup>20</sup>

It is generally agreed that the transition responsible for the Hartley band takes the molecule from its ground X<sup>1</sup>A<sub>1</sub> state to an electronically excited <sup>1</sup>B<sub>2</sub> state,<sup>21</sup> and the angular distribution of the fragments is consistent with this being a mainly parallel dissociation (the transition dipole moment lying in the molecular plane and perpendicular to the C<sub>2v</sub> axis), with dissociation of the bent molecule dominantly to O(<sup>1</sup>D) + O<sub>2</sub>(a<sup>1</sup>Δ<sub>g</sub>) being rapid in comparison with molecular rotation.<sup>22–28</sup> Around the maximum of the Hartley band (~250 nm) there are weak structures with a spacing of approximately 250 cm<sup>-1</sup>, as can be seen in Figure 1. The vibrational assignments of these peaks with classical techniques have been performed by Joens,<sup>29</sup> Parisse et al.,<sup>30</sup> and O'Keeffe et al.<sup>31</sup> using experimentally obtained absorption spectra<sup>17,30,32</sup> for the <sup>16</sup>O<sub>3</sub> and <sup>18</sup>O<sub>3</sub> stable isotopes. Those vibrational assignments in the Hartley band consist of combinations of the symmetric stretching mode  $\nu_1$  and bending mode  $\nu_2$ .

Another interpretation of the weak structures on the top of the Hartley band (~250 nm) is that mechanical nuclear motions on the <sup>1</sup>B<sub>2</sub> surface above the dissociation limit lead to the structure.<sup>33–46</sup> The structure corresponds to vibrational resonance states characterized by complex energies and probability decay over subpicosecond time periods. Each feature can be attributed to multiple resonance states which may overlap and be intrinsically unresolvable. In the corresponding classical picture of the dissociation, these resonances are associated with unstable periodic or almost periodic orbits which then return to the geometries of the Franck–Condon region at least once during the first 150 fs after photoabsorption.

The origin of the structured part of the Huggins band at wavelengths above about 310 nm has been the subject of debate.<sup>29,31,40,47–54</sup> Transitions are seen which support vibrational structure, but no distinct rotational lines can be observed, and the electronic parentage has been assigned as transitions to the same <sup>1</sup>B<sub>2</sub> state as for the Hartley band which supports bound vibrational levels below the threshold to the O(<sup>1</sup>D) + O<sub>2</sub>(a<sup>1</sup>Δ<sub>g</sub>) dissociation<sup>48,49</sup> or to bound vibrational levels of the second <sup>1</sup>A<sub>1</sub> state (2<sup>1</sup>A<sub>1</sub>) reached in a two-electron transition from the ground <sup>1</sup>A<sub>1</sub> (0,0,0) state but with an odd quantum number change in the antisymmetric stretch mode  $\nu_3$ , making the overall symmetry <sup>1</sup>B<sub>2</sub>,<sup>53</sup> and presumably gaining intensity from the nearby one photon <sup>1</sup>B<sub>2</sub> electronic state. The potential energy surface (PES) of the ground electronic state of O<sub>3</sub> has a bent structure with C<sub>2v</sub> symmetry ( $r_{12} = r_{23} = 2.42$  a<sub>0</sub>). The PES of the <sup>1</sup>B<sub>2</sub> state has a saddle point in the equinuclear distance region ( $r_{12} = r_{23}$ ) and two equivalent minima on this surface with C<sub>s</sub> symmetry in the exit valleys leading to the O(<sup>1</sup>D) + O<sub>2</sub>(a<sup>1</sup>Δ<sub>g</sub>) dissociation,<sup>21,55,56</sup>

while the PES of the  $2^1A_1$  state surface has been predicted to have a shallow minimum at  $r_{12} = r_{23}$  with  $C_{2v}$  symmetry at an energy approximately 0.5 eV below the minimum of the  $1B_2$  state and also correlates to the  $O(^1D) + O_2(a^1\Delta_g)$  dissociation channel.<sup>52,57</sup> The transition  $2^1A_1 \leftarrow X^1A_1$  is forbidden with regard to the dominant electronic configurations, while the transition to the  $1B_2$  states is fully allowed. Although Sinha et al.<sup>50</sup> presented rotational contours of the Huggins bands measured in supersonic jets and proposed assignments of the upper electronic state for the Huggins band, Takahashi et al.<sup>58</sup> did not observe any rotational contours of the Huggins band under essentially almost the same experimental conditions. Translational anisotropy measurements of photofragments provide information about the direction of the optical transition moment in the molecular coordinates.<sup>59</sup> However, in the case of the Huggins band, the translational anisotropy measurements are unable to distinguish between the two possibilities but are consistent with both; as positive values of the translational anisotropy factor  $\beta$  are predicted and measured by Hancock and co-workers.<sup>25,60,61</sup> Recently, O'Keeffe et al.<sup>31</sup> reanalyzed the assignments of the Huggins band vibrational structure with their photofragment excitation spectrum of  $O(^3P)$  for rotationally cooled ozone molecules in supersonic jets along with the absorption spectra measured previously with  $^{16}O_3$  and  $^{18}O_3$  stable isotopes at 195 K, and they attributed the upper electronic state of the Huggins band to the  $2^1A_1$  state. The recent theoretical study<sup>40</sup> has suggested that the Huggins and Hartley band systems are due to excitation to the same electronic state ( $1B_2$ ). Further experimental and theoretical studies are required to draw conclusions about the assignment of the upper electronic state for the Huggins band.

### 3. $O(^1D)$ Formation from the Photolysis of Ozone

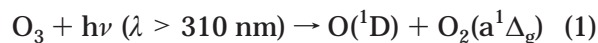
#### 3.1. $O(^1D)$ Formation in the Atmosphere

The source of  $O(^1D)$  in the lower atmosphere is the photolysis of ozone in the Hartley and Huggins bands. The ultraviolet photolysis of ozone in the strong Hartley band region (ca. 225–305 nm) mainly produces singlet oxygen atoms,  $O(^1D)$ , and singlet oxygen molecules with a quantum yield of about 0.9. The quantum yields of the  $O(^1D)$  atom formation from the ozone photolysis at wavelengths longer than 305 nm are strongly dependent on the photolysis wavelength and temperature. The strong increase in the ozone absorption cross section at wavelengths below 330 nm and the consequent absorption by overhead ozone leads to a sharp decrease of solar actinic flux becoming practically zero below 290 nm in the lower stratosphere and troposphere shown in Figure 2. Since photolysis of ozone in the lower atmosphere (<20 km) depends on the overlap of the wavelength dependent actinic flux and on the ozone absorption cross section, the opposing wavelength dependence of these two quantities essentially restricts the photodissociation to 290–330 nm.<sup>62</sup> This is precisely the wavelength region where  $O(^1D)$  production increases from near zero values around 330 nm to near unit

values around 290 nm. Therefore, the calculated atmospheric  $O(^1D)$  production rate is very sensitive to changes in the quantum yield for its production in the photolysis of ozone in this wavelength range. The atmospheric temperature between the lower stratosphere and the ground widely varies from 200 to 320 K. It is also this region where the UV absorption cross sections of ozone and the quantum yields for  $O(^1D)$  production are highly sensitive to the temperature. Thus, accurate definition of the quantum yields for  $O(^1D)$  production in ozone photolysis as a function of wavelength and temperature is essential for atmospheric chemistry.

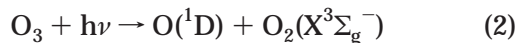
#### 3.2. $O(^1D)$ Quantum Yield Measurements

Until several years ago, based on many previous data sets, it was suggested that the  $O(^1D)$  production drops monotonically from near unity at  $\sim 290$  nm to zero by  $\sim 315$  nm,<sup>9,63–68</sup> since the wavelength threshold is around 310 nm for the energetically allowed channel



It was assumed that spin conservation would require that the coproduct of  $O(^1D)$  is  $O_2(^1\Delta)$ , since the upper state of ozone accessed by absorption in the strongly allowed transition is a singlet. However, the early laboratory data presented by Brock and Watson<sup>69</sup> and Trolrier and Wiesenfeld<sup>70</sup> in the 1980s indicated the presence of a “tail” in the  $O(^1D)$  quantum yield (i.e., a nonzero quantum yield) beyond this threshold. Adler-Golden et al.<sup>71</sup> pointed out that vibrationally excited ozone could generate  $O(^1D)$  via the spin-allowed channel (eq 1) well beyond the 310 nm energetic threshold calculated for the ground state of ozone, and in contrast to the early NASA/JPL recommendations,<sup>9</sup> an evaluation by Steinfeld et al.<sup>6</sup> recommended a “tail” in the  $O(^1D)$  yield which extended out to 325 nm. Ball et al.<sup>72</sup> reported quantum yield measurements of  $O_2(a^1\Delta)$  (the  $O(^1D)$  coproduct from the spin-allowed photodissociation of ozone) showing a tail that is very similar to that reported for  $O(^1D)$ . Michelsen et al.<sup>73</sup> further developed the concept of Adler-Golden et al.<sup>71</sup> and presented a model calculation that described the tail of the room-temperature  $O(^1D)$  quantum yield measured by Brock and Watson<sup>69</sup> and Trolrier and Wiesenfeld<sup>70</sup> and  $O_2(a^1\Delta)$  by Ball et al.<sup>72</sup> up to  $\sim 320$  nm. Their model assumed that the tail is due only to photolysis of vibrationally excited ozone; it did not take into account the spin-forbidden process, which was not known at that time. Their mathematical expression became the basis for the NASA/JPL recommendation in 1997.<sup>10</sup> Field experiments performed by Müller et al.<sup>74</sup> and Shetter et al.,<sup>75</sup> which compared  $J(O^1D)$  photolysis frequencies measured directly by a chemical actinometer with data obtained from solar actinic spectra and  $O(^1D)$  quantum yield spectra, were also consistent with the tail. Inclusion of the tail led to a much better agreement between measurements and calculations, as a function of solar zenith angle and total overhead ozone column.

The recent laboratory studies performed by Armerding et al.,<sup>76</sup> Takahashi et al.,<sup>77,78</sup> Ball et al.,<sup>79</sup> Silvente et al.,<sup>80</sup> Talukdar et al.,<sup>81</sup> Bauer et al.,<sup>82</sup> Smith et al.,<sup>83</sup> and Hancock and Tyley<sup>84</sup> have yielded new measurements of the O(<sup>1</sup>D) quantum yield as a function of wavelength and temperature with direct and indirect detection methods, showing clearly that the tail exists. More interestingly, some of these new measurements also show that the quantum yield does not go to zero even at wavelengths as long as ~330 nm when the temperature is cold enough to eliminate the existence of a significant fraction of vibrationally excited ozone. This nonzero yield has been attributed to the spin-forbidden channel for O(<sup>1</sup>D) production



and has now been clearly demonstrated via recent laboratory measurements by Takahashi et al.<sup>85</sup> and Denzer et al.<sup>60,61</sup> The significance of these changes in O(<sup>1</sup>D) quantum yields is very important to atmospheric calculations. Müller et al.<sup>74</sup> indicated that the tail contributes at least 30% of the noon-time J(O(<sup>1</sup>D)) value in summer in Jülich (solar zenith-angle = 28°) and that total integrated O(<sup>1</sup>D) production is enhanced by a factor of 1.38 due to the tail. The formation rate of O(<sup>1</sup>D) from the photolysis of ozone, J(O(<sup>1</sup>D)), is defined as follows

$$J(\text{O}(\text{}^1\text{D})) = \int_{\lambda} \sigma(\lambda, T) \Phi(\lambda, T) F(\lambda) d\lambda \quad (8)$$

where  $\sigma(\lambda, T)$  and  $\Phi(\lambda, T)$  are the absorption cross section of ozone and the O(<sup>1</sup>D) quantum yield at the photolysis wavelength  $\lambda$  and temperature  $T$  and  $F(\lambda)$  is the solar actinic flux. There are many situations in the atmosphere where the available wavelengths are restricted to greater than 310 nm. Such situations include high solar zenith angles and large overhead ozone columns, both common at high latitudes during late-Fall to early-Spring time. Talukdar et al.<sup>81</sup> suggested that for a solar zenith angle of 85°, the inclusion of the tail and the spin-forbidden dissociation process increase the J(O(<sup>1</sup>D)) value by a factor of 3.

### 3.3. Experimental Techniques for O(<sup>1</sup>D) Yield Measurements

The difficulties connected with the measurement of O(<sup>1</sup>D) quantum yields from the photolysis of ozone are primarily associated with the need for a narrow-band, widely tunable source of photolysis radiation, the difficulty of directly monitoring O(<sup>1</sup>D) spectroscopically, and the very large dynamic range (especially the ozone cross section) that the measurements span. For a given photolysis fluence and ozone concentration, the concentration of O(<sup>1</sup>D) produced varies by 6 orders of magnitude between 250 and 350 nm. In addition, the lifetime of O(<sup>1</sup>D) with respect to either reaction or quenching is extremely short in most common gases; exceptions are gases such as He, Ne, Ar, SF<sub>6</sub>, and CF<sub>4</sub>.<sup>2</sup>

Most of the recent measurements used some type of pulsed tunable laser as the photolysis light source. Such lasers provide a relatively high power and

narrow bandwidth source of tunable radiation. However, the variation in photolysis laser fluence, i.e., energy per unit area (or at least the relative values at different wavelengths), needs to be monitored accurately as the wavelength of the laser changes, and this measurement is not trivial. Since these lasers operate in the visible and require harmonic generation techniques to reach the UV, some changes in beam profile are unavoidable as the lasers are tuned. The study performed by Smith et al.<sup>83</sup> used broadband sources with bandwidths that varied between 0.05 and 4 nm.

O(<sup>1</sup>D) can be monitored by its emission O(<sup>1</sup>D) → O(<sup>3</sup>P) at 630 nm. This emission is both spin and electric dipole forbidden, and the radiative lifetime is 148 s. Nevertheless direct emission was used to monitor relative O(<sup>1</sup>D) quantum yields between 221 and 243.5 nm by Cooper et al.<sup>86</sup> Hancock and co-workers<sup>60,61,79,84</sup> applied (2+1) resonance-enhanced multiphoton ionization (REMPI) detection of O(<sup>1</sup>D) at 203.5 nm to O(<sup>1</sup>D) yield measurements between 305 and 330 nm, overcoming the interferences of the formation of O(<sup>1</sup>D) due to the photolysis of O<sub>3</sub> by the probe 203.5 nm laser pulse. The (2+1) excitation wavelength lies in a minimum in the UV absorption spectrum of O<sub>3</sub>. Laser-induced fluorescence (LIF), using single-photon excitation of the 3s <sup>1</sup>D<sub>2</sub><sup>0</sup>–2p <sup>1</sup>D<sub>2</sub> transition has been demonstrated by Takahashi et al.<sup>58,77,78,85</sup> This is technically the most demanding approach requiring sum frequency generation of vacuum ultraviolet (VUV) radiation with two tunable lasers. Nevertheless, it appears to offer high sensitivity, specificity, and no significant interference effects.

Because of the difficulties associated with direct observation of O(<sup>1</sup>D), many studies have utilized indirect detection, allowing the O(<sup>1</sup>D) to react with another molecule which is more easily monitored. Clearly the disadvantage of this approach is that it is indirect and O(<sup>1</sup>D) production is inferred rather than measured directly. Knowledge of the detailed chemistry associated with production of the “spectroscopic marker” is critical. Several studies have photolyzed O<sub>3</sub> in the presence of N<sub>2</sub>O. The reaction of O(<sup>1</sup>D) with N<sub>2</sub>O produces NO, which then undergoes further reaction with ozone, producing electronically excited NO<sub>2</sub>\* that can be detected by its chemiluminescence. This approach was used in several of the early studies.<sup>64,67–69,87,88</sup> A study by Trolier and Wiesenfeld<sup>70</sup> used energy transfer from O(<sup>1</sup>D) to CO<sub>2</sub> followed by detection of the infrared emission from vibrationally excited CO<sub>2</sub>.

Recently, three groups have monitored the OH produced by the reaction of O(<sup>1</sup>D) with water, H<sub>2</sub>, or methane. O(<sup>1</sup>D) reacts with H<sub>2</sub>O, H<sub>2</sub>, and CH<sub>4</sub> at rates which are close to the gas kinetic limit. Furthermore, H<sub>2</sub>O is very efficient at quenching vibrationally excited OH and does not “react” with vibrationally excited OH. Each study utilized LIF to monitor the OH, although they used different excitation schemes. Talukdar et al.<sup>81</sup> excited the A–X (1–0) transition at 282 nm monitoring (1–1) and (0–0) fluorescence at 308–315 nm. This detection scheme discriminates effectively against scattered probe laser light. Since the excitation transition lies within the

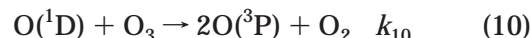
absorption spectrum of ozone, the probe beam generates some O(<sup>1</sup>D) atoms which can react within the time frame of the probe pulse to generate an interfering OH LIF signal. This increases the background or "noise" signal relative to the LIF signal from OH produced by the photolysis laser but introduces no complications. Armerding et al.<sup>76</sup> monitored the formation of OH in its ground vibrational level exciting the A–X (0–0) transition at 308 nm; in this scheme OH interference is reduced substantially but the excitation and detection wavelengths are similar. The reaction of O(<sup>1</sup>D) with H<sub>2</sub> and CH<sub>4</sub> produces OH with a substantial amount of vibrational excitation. Silvente et al.<sup>80</sup> and Bauer et al.<sup>82</sup> monitored OH ( $\nu = 1$ ) by exciting the A–X (0–1) transition at 351 nm and monitoring blue-shifted fluorescence at 308 nm. This approach minimizes noise and OH interference effects and allowed Bauer et al.<sup>82</sup> to monitor O(<sup>1</sup>D) yields out to 375 nm.

Smith et al.<sup>83</sup> used a combination of a monochromator and a Xe arc lamp for photolysis of N<sub>2</sub>O/O<sub>3</sub> mixtures with chemical ionization mass spectrometry (CIMS) detection of the NO<sub>2</sub> product. The NO molecule reacts with the O<sub>3</sub> and then produces NO<sub>2</sub>. The NO<sub>2</sub> is ionized by an ion–molecule reaction with O<sub>3</sub><sup>−</sup>. Finally, the NO<sub>2</sub><sup>−</sup> ion is detected with a quadrupole mass spectrometer. This method can distinguish O(<sup>1</sup>D) from O(<sup>3</sup>P) without using any laser system. Also, unlike the previous studies that utilized the O(<sup>1</sup>D) + N<sub>2</sub>O reaction, vibrationally excited NO should not be a problem since NO<sub>2</sub> was detected directly and all the NO (ground and vibrationally excited) was converted rapidly to NO<sub>2</sub>. Their observation of the "tail" confirms that this is not an artifact produced by the high peak power associated with laser photolysis.

### 3.4. Absolute Values of the O(<sup>1</sup>D) Quantum Yield

Absolute measurements of O(<sup>1</sup>D) quantum yields at room temperature have been presented by Talukdar et al.<sup>89</sup> at photolysis wavelengths of 248 and 308 nm, by Takahashi et al.<sup>77,78</sup> at 308 nm, by Greenblatt and Wiesenfeld<sup>90</sup> at 248 and 308 nm, by Amimoto et al.<sup>91</sup> at 248 nm, by Brock and Watson<sup>92</sup> at 266 nm, and by Turnipseed et al.<sup>93</sup> at 222 and 193 nm. Results are listed in Table 2. The latest recommendation of the O(<sup>1</sup>D) quantum yield for atmospheric modeling is based on the absolute quantum yield values at 308 nm as described elsewhere.<sup>94</sup> Since the photolysis of ozone at wavelengths longer than 300 nm is of importance in atmospheric chemistry, the absolute measurements at 308 nm are of most atmospheric significance. Two types of experimental methods were

used for the measurements of the absolute yield at 308 nm. Talukdar et al.<sup>89</sup> and Greenblatt and Wiesenfeld<sup>90</sup> measured the time profile of O(<sup>3</sup>P) resonance fluorescence after the pulsed laser photodissociation of O<sub>3</sub>. The temporal profile of O(<sup>3</sup>P) initially jumps due to direct formation in the photolysis of O<sub>3</sub>; the initial jump is followed by an exponential rise controlled by the following reactions of O(<sup>1</sup>D) and a slow decay due to diffusion.



On the basis of experimental results that the two rate coefficients are equal ( $k_9/k_{10} = 1.0$ ),<sup>10,89</sup> the absolute O(<sup>1</sup>D) quantum yield value was calculated from amounts of the initial jump and the exponential rise of the O(<sup>3</sup>P) signal. On the other hand, Takahashi et al.<sup>77,78</sup> measured photofragment yield spectra of both O(<sup>3</sup>P) and O(<sup>1</sup>D) after the photolysis of O<sub>3</sub> by scanning the photolysis laser wavelength between 308 and 326 nm and monitoring the O(<sup>3</sup>P) and O(<sup>1</sup>D) concentration with a VUV laser-induced fluorescence technique. The sum of the photofragment yield spectra for both O(<sup>1</sup>D) and O(<sup>3</sup>P)<sub>*i*</sub> atoms with absolute scales should correspond to the absorption spectrum of the O<sub>3</sub> molecule.

$$\sigma_{\text{abs}}(\lambda) = s_{1\text{D}}Y_{1\text{D}}(\lambda) + s_{3\text{P}}Y_{3\text{P}}(\lambda) \quad (11)$$

where  $\sigma_{\text{abs}}(\lambda)$  is the absorption cross section of O<sub>3</sub> at wavelength  $\lambda$ ,  $Y_{1\text{D}}(\lambda)$  and  $Y_{3\text{P}}(\lambda)$  are the experimentally obtained photofragment yield spectra of O(<sup>1</sup>D) and O(<sup>3</sup>P)<sub>*i*</sub>, and  $s_{1\text{D}}$  and  $s_{3\text{P}}$  are the detection sensitivity factors for O(<sup>1</sup>D) and O(<sup>3</sup>P)<sub>*i*</sub>, respectively. In this relationship, the sum of the quantum yields for nascent O(<sup>1</sup>D) and O(<sup>3</sup>P) atoms is assumed to be equal to unity. The threshold wavelength for the dissociation to 3O(<sup>3</sup>P) is 198 nm. The lifetime of the upper electronic state of ozone is estimated to be less than a few picoseconds,<sup>58</sup> which is too short to generate any fluorescence. Therefore, the assumption of unity dissociation yield for the sum of the O(<sup>3</sup>P) and O(<sup>1</sup>D) fragments seems to be reasonable. Since the yield spectra of O(<sup>1</sup>D) and O(<sup>3</sup>P) are not parallel in the wavelength range of 308–328 nm, a pair of the  $s_{1\text{D}}$  and  $s_{3\text{P}}$  values were determined so that the sum of  $s_{1\text{D}}Y_{1\text{D}}(\lambda)$  and  $s_{3\text{P}}Y_{3\text{P}}(\lambda)$  reproduced the absorption spectrum  $\sigma_{\text{abs}}(\lambda)$ . The absolute value of O(<sup>1</sup>D) quantum yield is calculated as  $\Phi(\lambda) = s_{1\text{D}}Y_{1\text{D}}(\lambda)/\sigma_{\text{abs}}(\lambda)$ .

As listed in Table 2, the published absolute values of O(<sup>1</sup>D) quantum yields at 308 nm using the two

**Table 2. Results of the Measurements of Absolute O(<sup>1</sup>D) Quantum Yields in the Photolysis of Ozone**

wavelength (nm)	absolute O( <sup>1</sup> D) quantum yield	stated error	method	ref
308	0.79	±0.10	time profile of O( <sup>3</sup> P) resonance fluorescence intensity	Talukdar et al. <sup>89</sup>
308	0.79	±0.12	photofragment excitation spectra for O( <sup>3</sup> P) and O( <sup>1</sup> D) by VUV-LIF	Takahashi et al. <sup>77,78</sup>
308	0.79	±0.02	time profile of O( <sup>3</sup> P) resonance fluorescence intensity	Greenblatt and Wiesenfeld <sup>90</sup>
266	0.88	±0.02	time profile of O( <sup>3</sup> P) resonance fluorescence intensity	Brock and Watson <sup>92</sup>
248	0.91	±0.06	time profile of O( <sup>3</sup> P) resonance fluorescence intensity	Talukdar et al. <sup>89</sup>
248	0.94	±0.01	time profile of O( <sup>3</sup> P) resonance fluorescence intensity	Greenblatt and Wiesenfeld <sup>90</sup>
248	0.85	±0.02	time profile of O( <sup>3</sup> P) resonance fluorescence intensity	Amimoto et al. <sup>91</sup>

different experimental techniques at room temperature are in good agreement. The quoted uncertainty from the different studies (see Table 2) is in the range 0.02–0.12. The uncertainty estimate of 0.02 by Greenblatt and Wiesenfeld<sup>90</sup> seems to be too small given their assumption that  $k_9/k_{10} = 1.0$ . Additional work to determine more accurately the absolute value of  $O(^1D)$  quantum yield at 308 nm is needed, since this value affects the overall accuracy of the yields at other wavelengths.

### 3.5. $O(^1D)$ Quantum Yield between 306 and 328 nm

Because the changes in the  $O(^1D)$  quantum yields have been reported only recently as described in section 3.2, a panel of seven scientists working in the area of ozone photodissociation has been organized to evaluate the quantum yields for  $O(^1D)$  production in ozone photolysis at wavelengths between 308 and 328 nm since 1999. This is a part of the joint activity of two international research projects, Stratospheric Processes And their Role in Climate (SPARC) and International Global Atmospheric Chemistry (IGAC). The aim of the panel is to critically evaluate the data available to date and to develop the best possible data set for atmospheric modeling. The first results of the panel activity has been published very recently by Matsumi et al.<sup>94</sup> and also can be accessed from the SPARC Data Center website (<http://www.sparc.sunysb.edu/html/RefData.html>) with the supplementary data. The latest assessments of kinetic and photochemical data for atmospheric chemistry by the IUPAC subcommittee<sup>8</sup> and the latest recommendation data published by NASA/JPL (2003)<sup>12</sup> have adopted the results of the above panel for the quantum yields for  $O(^1D)$  production in ozone photolysis at UV wavelengths.

To obtain a wavelength dependence of the  $O(^1D)$  yield at 298 K in the wavelength range of 306–328 nm, the panel selected the recent experimental data sets reported by eight groups are used, Talukdar et al.,<sup>81</sup> Takahashi et al.,<sup>77</sup> Ball et al.,<sup>79</sup> Armerding et al.,<sup>76</sup> Bauer et al.,<sup>82</sup> Brock and Watson,<sup>69</sup> Trolier and Wiesenfeld,<sup>70</sup> and Smith et al.<sup>83</sup> The panel renormalized the data sets to reduce the systematic error before averaging them. The renormalization factors for the data sets were chosen to achieve the best consistency among the yield curves over the full 307–320 nm wavelength range. The average of the data sets was then scaled to the value of 0.79 at 308 nm. The renormalized values of the data sets reported by eight groups, and their average values are plotted in Figure 3.

To obtain the parameters for the expression to calculate the recommended values in the ranges of  $T = 200$ – $320$  (K) and  $\lambda = 306$ – $328$  (nm), the panel used the experimental data of the temperature dependence reported by five groups, Talukdar et al.,<sup>81,89</sup> Takahashi et al.,<sup>78</sup> Hancock et al.,<sup>84</sup> Bauer et al.,<sup>82</sup> and Smith et al.,<sup>83</sup> as well as the above averaged data at 298 K. The  $O(^1D)$  quantum yields at 308 nm are also dependent on the temperature of parent ozone molecules. First, the panel examined the temperature dependence of the  $O(^1D)$  yield at 308 nm.

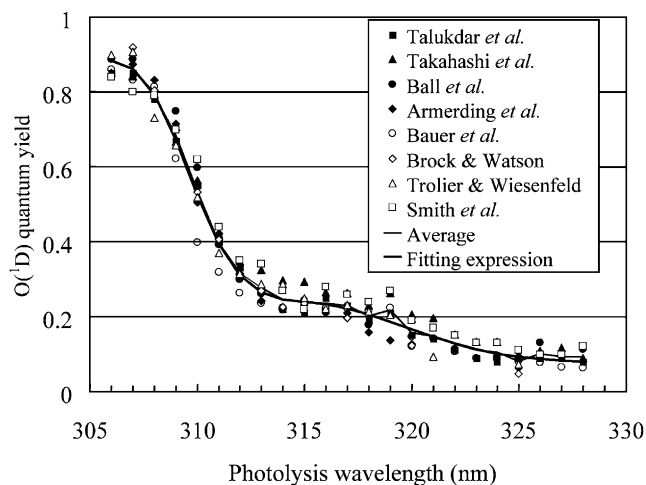


**Figure 3.** Wavelength dependence of the  $O(^1D)$  quantum yield in the photolysis of  $O_3$  at 298 K. The renormalized values of the data sets reported by eight groups and their average values are plotted. The renormalization factor is 1.00 for the data set by Talukdar et al.,<sup>81</sup> 1.00 for Takahashi et al.,<sup>77</sup> 0.93 for Ball et al.,<sup>79</sup> 1.05 for Armerding et al.,<sup>76</sup> 1.03 for Bauer et al.,<sup>82</sup> 1.05 for Brock and Watson,<sup>69</sup> 0.93 for Trolier and Wiesenfeld,<sup>70</sup> and 1.00 for Smith et al.<sup>83</sup> The recommendation values calculated with eq 13 for 298 K in the text is also plotted. (Reprinted with permission from ref 94. Copyright 2002 American Geophysical Union.)

The linear least-squares fitting to the detailed experimental results at 308 nm assuming a quantum yield of 0.79 at 298 K leads to the equation<sup>94</sup>

$$\Phi(308 \text{ nm}, T) = (6.10 \times 10^{-4})T + 0.608 \quad (12)$$

where  $\Phi(308 \text{ nm}, T)$  is the quantum yield at 308 nm and temperature  $T$  in Kelvin. The experimental data at temperatures other than 298 K, reported by the above five groups, is normalized to  $\Phi(308 \text{ nm})$  calculated from this expression.

For the fitting expression that presents the wavelength and temperature dependence of the  $O(^1D)$  quantum yield, the panel used an equation containing three Gaussian-like functions, a temperature term, and a constant term<sup>12,94</sup>

$$\Phi(\lambda, T) = \left( \frac{q_1}{q_1 + q_2} \right) \times A_1 \times \exp \left\{ - \left( \frac{X_1 - \lambda}{\omega_1} \right)^4 \right\} + \left( \frac{q_2}{q_1 + q_2} \right) \times A_2 \times \left( \frac{T}{300} \right)^2 \times \exp \left\{ - \left( \frac{X_2 - \lambda}{\omega_2} \right)^2 \right\} + A_3 \times \left( \frac{T}{300} \right)^{1.5} \times \exp \left\{ - \left( \frac{X_3 - \lambda}{\omega_3} \right)^2 \right\} + c \quad (13)$$

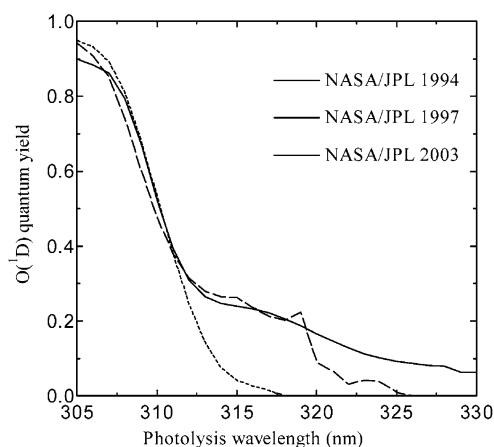
where

$$q_i = \exp \left( - \frac{\nu_i}{RT} \right) \quad (14)$$

and  $X_{1-3}$ ,  $A_{1-3}$ ,  $\omega_{1-3}$ ,  $\nu_2$ , and  $c$  are fitting parameters,  $\lambda$  is in nm,  $T$  is in K, and values of  $\nu_1$  and  $R$  are 0 ( $\text{cm}^{-1}$ ) and 0.695 ( $\text{cm}^{-1}/\text{K}$ ), respectively. The values of the parameters were obtained by fitting the expression to the experimental data using a nonlinear least-squares method.<sup>94</sup> The obtained best-fit parameters are listed in Table 3. The calculated yield

**Table 3. Parameters for the Eq 13 in the Text To Calculate Recommendation Values of O(<sup>1</sup>D) Quantum Yields<sup>12,94</sup>**

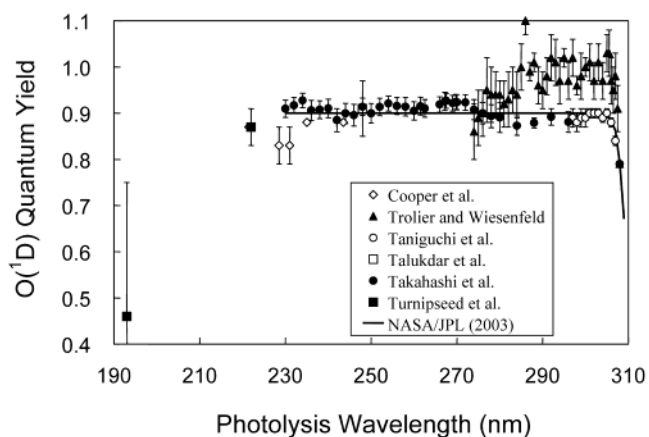
	$i = 1$	$i = 2$	$i = 3$
$X_i$ (nm)	304.225	314.957	310.737
$\omega_i$ (nm)	5.576	6.601	2.187
$A_i$	0.8036	8.9061	0.1192
$\nu_1$ (cm <sup>-1</sup> )	0	825.518	
$c$	0.0765		

**Figure 4.** Comparison of the recommendation values of O(<sup>1</sup>D) quantum yields at 298 K in the wavelength range 305–330 nm: NASA/JPL (1994),<sup>9</sup> NASA/JPL (1997),<sup>10</sup> and NASA/JPL (2003).<sup>12</sup> NASA/JPL (2003)<sup>12</sup> have adopted the results of the evaluation panel (2002)<sup>94</sup> for the quantum yields of O(<sup>1</sup>D) (eq 13 in the text with the fitting parameter in Table 3). (Adapted from ref 94. Copyright 2002 American Geophysical Union.)

curves at temperatures of 298 K are plotted in Figure 3 for comparison with the experimental data. The comparisons of the values calculated at 298 K using the expressions presented by the NASA/JPL 1994, 1997, and 2003 recommendations<sup>9,10,12</sup> are shown in Figure 4. NASA/JPL (2003)<sup>12</sup> adopted the results of the evaluation panel (2002)<sup>94</sup> for the quantum yields of O(<sup>1</sup>D). The evaluation panel indicated that at room temperature (298 K) the uncertainties of the quantum yield values calculated with expression 13 have been estimated  $\pm 10\%$  ( $1\sigma$ ) for  $\Phi(\lambda, 298 \text{ K}) \geq 0.4$ , while the uncertainties have been estimated to be  $\pm 0.04$  in the absolute value for  $\Phi(\lambda, 298 \text{ K}) < 0.4$ . At temperatures other than room temperature, the uncertainties of the yield have been estimated to be  $\pm 15\%$  for  $\Phi(\lambda, T) \geq 0.4$  and  $\pm 0.06$  for  $\Phi(\lambda, T) < 0.4$ .<sup>94</sup>

### 3.6. O(<sup>1</sup>D) Quantum Yield below 306 nm and above 328 nm

For the wavelength range of 290–305 nm, the value of 0.95 has been recommended by NASA/JPL 1997.<sup>10</sup> However, recent experimental studies reported by Talukdar et al.,<sup>81</sup> Taniguchi et al.,<sup>95</sup> and Takahashi et al.<sup>96</sup> indicated that the O(<sup>1</sup>D) yield values in the wavelength range of 290–305 nm is around 0.90, using the reference yield value of 0.79 at 308 nm. Talukdar et al.<sup>81</sup> reported the yield values do not depend on the temperature of O<sub>3</sub> in this wavelength range. The evaluation panel has recommended the yield of 0.90 in the range of 290–305 nm

**Figure 5.** Quantum yield values for O(<sup>1</sup>D) formation in the Hartley band photolysis of ozone at room temperature as a function of photolysis wavelength. Original data presented by Cooper et al.,<sup>86</sup> Trolier and Wiesenfeld,<sup>70</sup> Taniguchi et al.,<sup>95</sup> Talukdar et al.,<sup>81</sup> Takahashi et al.,<sup>96</sup> Turnipseed et al.,<sup>93</sup> and NASA/JPL (2003)<sup>12</sup> are plotted.

with uncertainties of  $\pm 0.09$ , which is independent of the temperature.<sup>94</sup>

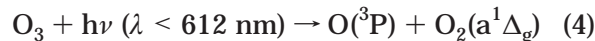
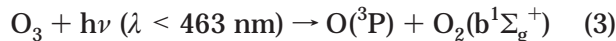
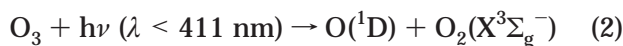
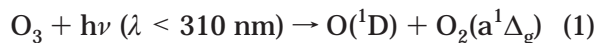
For the wavelength range of 220–290 nm, the absolute yield at 248 nm is reported to be  $0.91 \pm 0.06$  by Talukdar et al.<sup>81</sup> and  $0.94 \pm 0.01$  by Greenblatt and Wiesenfeld,<sup>90</sup> while the yield at 266 nm is  $0.88 \pm 0.02$  by Brock and Watson<sup>92</sup> as listed in Table 2. Cooper et al.<sup>86</sup> observed weak 630-nm fluorescence from the spin-forbidden O(<sup>1</sup>D)  $\rightarrow$  O(<sup>3</sup>P) transition in the photolysis of O<sub>3</sub> between 221 and 243.5 nm and determined the O(<sup>1</sup>D) quantum yields, using the reference yield values at 248 and 266 nm. They indicated the O(<sup>1</sup>D) quantum yield was almost constant in this wavelength range. Most recently, Takahashi et al.<sup>96</sup> reported the O(<sup>1</sup>D) quantum yield at  $297 \pm 2 \text{ K}$  as a function of the photolysis wavelength between 230 and 300 nm, using the O(<sup>1</sup>D) quantum yield value of 0.79 at 308 nm as a reference. Turnipseed et al.<sup>93</sup> studied the photodissociation reaction of O<sub>3</sub> at both 222 and 193 nm by means of the resonance fluorescence detection of O(<sup>3</sup>P) atoms with an atomic resonance lamp. They reported the quantum yields for O(<sup>3</sup>P) and O(<sup>1</sup>D) formation from 193 nm photolysis to be  $0.57 \pm 0.14$  and  $0.46 \pm 0.29$ , respectively. Stranges et al.<sup>97</sup> photolyzed an ozone molecular beam at 193 nm and measured the kinetic energy release and recoil anisotropy of atomic oxygen fragments using an electron bombardment quadrupole mass spectrometer with an angle-resolved time-of-flight technique. They estimated the branching ratios to be  $16.8 \pm 1.5\%$  for O(<sup>3</sup>P) + O<sub>2</sub>(X<sup>3</sup>Σ<sub>g</sub><sup>-</sup>),  $45.5 \pm 2.5\%$  for O(<sup>1</sup>D) + O<sub>2</sub>(a<sup>1</sup>Δ<sub>g</sub>),  $23.3 \pm 2.0\%$  for O(<sup>1</sup>D) + O<sub>2</sub>(b<sup>1</sup>Σ<sub>g</sub><sup>+</sup>),  $7.7 \pm 0.6\%$  for O(<sup>3</sup>P) + O<sub>2</sub>(X<sup>3</sup>Σ<sub>g</sub><sup>-</sup>), and  $2.0 \pm 0.2\%$  for 3O(<sup>3</sup>P) from the analysis of the translational energy distributions. The IUPAC subcommittee<sup>8</sup> recommended a constant value of 0.90 for  $220 < \lambda < 305 \text{ nm}$ , while NASA/JPL (2003)<sup>12</sup> recommended a constant value of 0.90 for  $\lambda < 306 \text{ nm}$ . Figure 5 shows these O(<sup>1</sup>D) quantum yield data in the wavelength range of 193–308 nm.

Even at the wavelength longer than 328 nm, the O(<sup>1</sup>D) quantum yield does not drop to zero. The formation of O(<sup>1</sup>D) is attributed to the spin-forbidden

dissociation to  $O(^1D) + O_2(X^3\Sigma_g^-)$ , channel 2, as will be described later. The energetic threshold for this spin-forbidden process (eq 2) is around 411 nm. This implies that the formation of  $O(^1D)$  can continue to 411 nm. Bauer et al.<sup>82</sup> measured the relative  $O(^1D)$  yield up to 370 nm. They proposed an  $O(^1D)$  yield of  $0.064 \pm 0.006$  between 325 and 375 nm. Smith et al.<sup>83</sup> reported the quantum yields are nearly constant ( $\sim 0.12$ ) and independent of temperature between 328 and 338 nm. In the wavelength range of 329–340 nm, the evaluation panel recommend the value of  $0.08 \pm 0.04$ , which is independent of the temperature. The  $J(O(^1D))$  value is still sensitive to the  $O(^1D)$  quantum yields around 330 nm at large solar zenith angles. Therefore, more measurements are needed with various experimental techniques around 330–340 nm. The  $O(^1D)$  formation in the atmosphere above 340 nm is not significant due to the small absorption coefficient of  $O_3$ .

### 3.7. Physical Processes of $O(^1D)$ Formation

It is important to understand the physical processes underlying the behaviors of the  $O(^1D)$  quantum yield in the photolysis of ozone as functions of wavelength and temperature. There are five energetically possible fragmentation pathways in the UV–vis photolysis of  $O_3$



For photodissociation in the Hartley band at  $\lambda < 300$  nm, it has generally been accepted that channels 1 and 5 are predominant, with reported quantum yields of ca. 0.9 and 0.1, respectively, as described in the previous section. As indicated before, the spin-forbidden channel (eq 2) occurs in the UV region above 300 nm as well as spin-allowed channels 1 and 5. Production of the  $O(^1D)$  atoms above 310 nm has been attributed to both channel 1 via the photodissociation of internally excited  $O_3$  and the spin-forbidden dissociation channel 2. The contributions made by these excitation processes to the quantum yields for  $O(^1D)$  atoms from  $O_3$  photolysis are schematically indicated in Figure 6. These excitation processes are schematically shown in Figure 7.

#### 3.7.1. Photodissociation of Vibrationally Excited Ozone

Taniguchi et al.<sup>98</sup> reported the precise bond energy for the dissociation channel 1,  $O(^1D) + O_2(a^1\Delta_g)$ , to be  $386.59 \pm 0.04 \text{ kJ mol}^{-1}$ , and the standard heat of formation of  $O_3$  at 0 K is calculated to be  $\Delta_f H^\circ(O_3) = -144.31 \pm 0.14 \text{ kJ mol}^{-1}$  by observing the cutoff point in the  $O(^1D)$  photofragment excitation spectrum of the rotationally cooled ozone in a supersonic jet and by measuring the translational energy of  $O(^1D)$  with

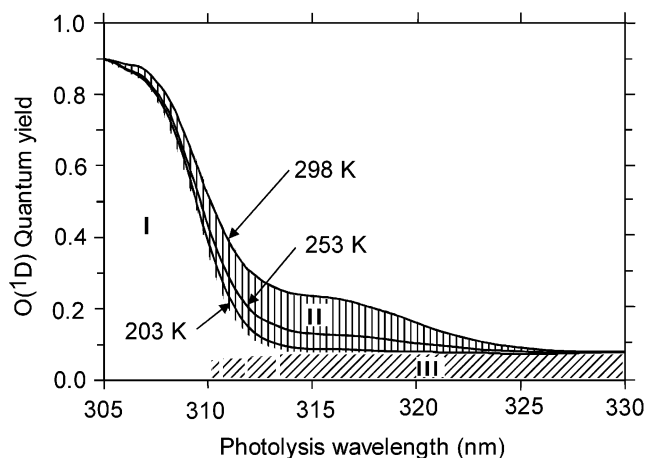


**Figure 6.** Recommendation values of  $O(^1D)$  quantum yields calculated with eq 13 in the text with the fitting parameter in Table 3 for 203, 253, and 298 K in the wavelength range 305–330 nm (solid lines). Contributions made by the various dissociation processes to the quantum yields for  $O(^1D)$  atoms from  $O_3$  photolysis are also indicated. Region I corresponds to the  $O(^1D)$  formation following excitation of parent vibration less molecules and dissociation via channel 1,  $O(^1D) + O_2(a^1\Delta_g)$ . Region II (hatched with vertical lines) indicates the contribution from the hot band excitation process leading to  $O(^1D)$  formation via channel 1,  $O(^1D) + O_2(a^1\Delta_g)$ , at 298 K, while region III (hatched with slash lines) represents the contribution from the spin-forbidden process leading to  $O(^1D)$  formation via channel 2,  $O(^1D) + O_2(X^3\Sigma_g^-)$ . (Reprinted with permission from ref 94. Copyright 2002 American Geophysical Union.)

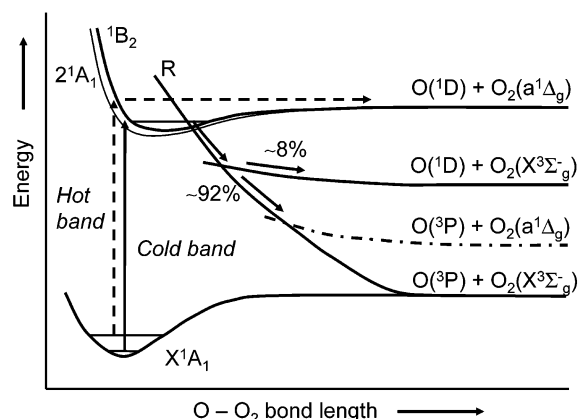


**Figure 7.** Schematic diagram of the potential curves as a function of dissociation coordinate, with the possible dissociation channels indicated. The energies of the vibrationally excited molecule are not shown to scale and serve to illustrate excitation to form  $O(^1D)$  and  $O_2(a^1\Delta_g)$  products from hot band excitation at photon energies where process 1 is energetically forbidden for the ground vibrational state.

a two-dimensional product imaging technique. This corresponds to a wavelength limit at 0 K of  $309.44 \pm 0.02 \text{ nm}$  (in a vacuum wavelength) for channel 1. Production of  $O(^1D)$  atoms at  $\lambda > 309.45 \text{ nm}$ , however, was observed in the flow cell experiments at 200–320 K,<sup>78,81–83</sup> and the temperature-dependent part of the quantum yield has been attributed to the photodissociation of vibrationally excited parent  $O_3$ . The energy difference in the threshold energies for the cold and hot band was measured to be  $1056 \pm 20 \text{ cm}^{-1}$  from the difference in the threshold photolysis wavelengths in supersonic free jet experiments,<sup>58</sup>

which is equal to the vibrational spacing for the antisymmetric stretching  $\nu_3$  vibration of  $O_3(X^1A_1)$ ,  $1042\text{ cm}^{-1}$ ,<sup>99</sup> within experimental error (the  $\nu_1$  and  $\nu_2$  levels are at  $1103$  and  $701\text{ cm}^{-1}$ ), and therefore the active vibrational mode in the hot band excitation is thus assigned to the antisymmetric vibration. The thermal population in the  $\nu_3'' = 1$  level of  $O_3(X^1A_1)$  is calculated to be only 0.6% of that of the  $\nu'' = 0$  level at room temperature, but the Franck–Condon (FC) factor for the vibrational transition is suggested to be more than several tens of times larger for the  $\nu_3'' = 1$  level than for the  $\nu'' = 0$  level because of preferential overlap of the potential surfaces of the ground and excited states.<sup>58</sup> The upper electronic state for the hot band excitation should be identical with that for the Hartley system, which is assigned to be the  $^1B_2-X^1A_1$  transition. On the basis of ab initio calculations,<sup>21,51,52,100</sup> the potential energy surface of the  $^1B_2$  state is of  $C_s$  symmetry and there are shallow double minima at the asymmetric bond lengths,  $r_{12} = 2.9\text{--}3.1\text{ a}_0$  and  $r_{23} = 2.3\text{--}2.4\text{ a}_0$ , for a bond angle of  $116^\circ$  which is the equilibrium angle in the  $X^1A_1$  state. It was reported that the energy barrier along the  $r_{12} = r_{23}$  diagonal is more than 1 eV higher than the exit channel to  $O(^1D) + O_2(a^1\Delta_g)$ .<sup>100</sup> Since the electronic ground-state  $X^1A_1$  has a symmetric geometry ( $r_{12} = r_{23} = 2.42\text{ a}_0$ ), the transition moment from the ground state to the double minimum potential state may be extensively induced by excitation in the antisymmetric vibration mode due to favorable FC factors. Therefore, it is reasonable that the antisymmetric stretching mode is active in the hot band excitation resulting in the dissociation to  $O(^1D) + O_2(a^1\Delta_g)$ . The theoretical absorption spectrum calculated by Adler-Golden<sup>101</sup> indicated that the  $\nu_3$  band excitation largely enhanced the absorption cross sections in the longer wavelength side of the Hartley band using the potential surfaces calculated by Hay and Dunning,<sup>21</sup> while the  $\nu_1$  and  $\nu_2$  band excitation did not enhance the absorption cross section very much. Adler-Golden et al.<sup>71</sup> found that the experimental absorption spectrum of the  $\nu_3$  band excited ozone produced by  $CO_2$  laser irradiation induced the enhancement of the absorption intensity in the red wavelength side of the Hartley band and predicted the large temperature dependence of the  $O(^1D)$  quantum yield in the wavelength region of  $308\text{--}322\text{ nm}$ . Zittel and Little<sup>102</sup> measured the  $O(^1D)$  formation yields in the UV photodissociation of ozone around  $310\text{ nm}$  with and without  $CO_2$  laser irradiation which was tuned to the  $\nu_3$  band of ozone and found that the photodissociation cross section for production of  $O(^1D)$  increased by nearly 2 orders of magnitude with the IR excitation of the  $\nu_3$  band at a photolysis wavelength of  $314.5\text{ nm}$ .

### 3.7.2. Spin-Forbidden Processes

In the Huggins band region there is clear evidence for the existence of a spin-forbidden channel forming  $O(^1D)$ . Measurements of the translational energy distributions of the  $O(^1D)$  fragments have shown that they contain contributions from species formed with kinetic energies well above those possible on energetic grounds from channel 1,  $O(^1D) + O_2(a^1\Delta_g)$ , and are entirely consistent with those expected from

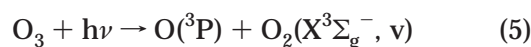
channel 2,  $O(^1D) + O_2(X^3\Sigma_g^-)$ .<sup>60,61,85</sup> The temperature-independent part of the quantum yield above  $320\text{ nm}$  is attributed to the spin-forbidden channel 2. At the photolysis wavelength of  $313\text{ nm}$  it can still be distinguished from the spin-allowed step.<sup>61</sup> The approximate constancy of the quantum yield for the lowest temperature data at wavelengths longer than  $313\text{ nm}$  suggests that there is a persistent spin-forbidden yield at about the 8% level at wavelengths longer than  $313\text{ nm}$  at all temperatures. The contributions of the spin-forbidden process at the wavelengths shorter than  $313\text{ nm}$  have not been revealed.

Since the photoexcited state of ozone is a singlet state even at the photolysis wavelengths where the spin-forbidden product pair,  $O(^1D) + O_2(X^3\Sigma_g^-)$ , is produced, the photoabsorption would be followed by a curve crossing to a dissociative triplet state. Lifetimes of the states reached by absorption in the structured bands are seen to increase with increasing wavelength in measurements of both line widths<sup>58</sup> and translational anisotropies.<sup>61</sup> This observation is consistent with an energy-dependent intersystem crossing rate and would not be expected for direct absorption to a dissociative triplet state.

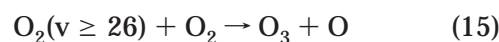
## 4. Implications for Atmospheric Chemistry

### 4.1. Formation $O_2(v)$ in the Photolysis of Ozone and Subsequent Reactions

The role of vibrationally excited molecules,  $O_2(v)$ , in atmospheric chemistry is an issue that has been debated. It has been established that when ozone is photodissociated in the Hartley band, there is a triplet channel with a yield of  $\sim 0.1$  by observations of nascent  $O(^3P)$  atoms.<sup>22,69,89,90,91,96,103–105</sup>



This is a spin-allowed dissociation process. The  $O_2(X^3\Sigma_g^-)$  fragment, the counterpart of the  $O(^3P)$  products, can have a lot of internal energy after the photodissociation, since the excess energy of this channel can be large when the ozone is photodissociated in the UV region.<sup>105–109</sup> Actually, vibrational excited  $O_2(X^3\Sigma_g^-)$  molecules,  $O_2(v)$ , have been directly observed after the photodissociation of ozone using a laser-induced fluorescence technique.<sup>105,107,110,111</sup> Models of stratospheric chemistry underpredicted the ozone concentrations. This difference between the model calculation and field measurement is called the “ozone-deficit problem”.<sup>112–114</sup> Attempts to account for this discrepancy have been explained by a new ozone source involving the  $O_2(v)$  molecules produced by the UV photodissociation of ozone.<sup>105,115–117</sup> The vibrational states of the oxygen atoms produced in the UV photolysis of ozone in the stratosphere can be under nonthermodynamic equilibrium (non-LTE) conditions. It was suggested that highly vibrationally excited molecular oxygen react with thermally equilibrated  $O_2$  to form ozone and atomic oxygen

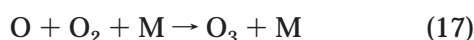
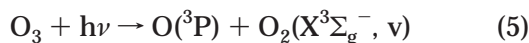


Experimental studies in which highly vibrationally

excited  $O_2$  was produced directly by stimulated emission pumping demonstrated what appeared to be anomalously efficient collisional deactivation by molecular oxygen of  $O_2(v=26, 27)$ , a result that was interpreted to indicate that such deactivation resulted in production of odd oxygen in reaction 15.<sup>116,118</sup> This mechanism is based on autocatalytic production of odd oxygen species following ozone photodissociation at wavelengths below 243 nm.<sup>105</sup> A bimodal  $O(^3P)$  translational energy distribution was seen following ozone photodissociation at 226 nm, implying the coincident production of triplet  $O_2$  containing  $>4$  eV internal energy.<sup>105</sup> Subsequent observation of highly vibrationally excited  $O_2$  following UV photolysis of  $O_3$  further suggested that this photolysis initiates the ozone formation reaction 15, leading to significant additional production of odd oxygen in the stratosphere and hence explain the ozone-deficit problem. Since ozone in the stratosphere dissociates and recombines many times before any new ozone formed or lost by the Chapman mechanism, a small quantum yield for reaction 15 may have a significant impact on the ozone budget. Although the quantum yield for the production of  $O_2(v \geq 26)$  by photodissociation (eq 5) was found to be only 0.8% at 226 nm, the process was estimated to produce odd oxygen at levels up to 48% that of the Chapman mechanism in 2-dimensional atmospheric models.<sup>105,117</sup>

Since this ozone formation mechanism has not been fully explained experimentally due to a lack of direct evidence that  $O_3$  is formed through reaction 15, the caveat extends to theoretical studies.<sup>119–126</sup> None of those theoretical studies provided the evidence for the formation of ozone in reaction 15, although the relevance of nonadiabatic processes has been debated.<sup>126,127</sup> Furthermore, the recent study on the comparisons between the model calculations and observation results in the stratosphere<sup>128</sup> reported that there was no evidence of the ozone-deficit problem owing to higher quality atmospheric data and improved laboratory measurements of rate coefficients without including new ozone formation processes such as  $O_2(v) + O_2$ .

Another mechanism for the new atmospheric  $O_3$  production source in the stratosphere was proposed by Slanger et al.<sup>129</sup> They suggested that the  $O_2(v)$  molecules absorb another 248 nm photon and dissociate to the O atoms through hot band excitation of the  $O_2(B^3\Sigma_u^- - X^3\Sigma_g^-)$  Schumann–Runge (SR) system which is the well-known strong absorption band of the ground-state  $O_2$  in the vacuum UV wavelength region ( $<195$  nm), since it was discovered that irradiation of  $O_2$  at the KrF excimer laser wavelength of 248 nm produced ozone.<sup>129</sup> The produced O atoms generate ozone molecules by the reaction with other  $O_2$  molecules.

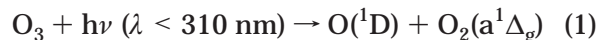


Toumi<sup>130</sup> suggested that this mechanism increased

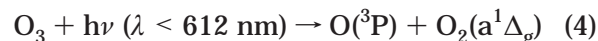
in the model ozone concentrations up to 40% in the upper stratosphere. However, Slanger and co-workers indicated that the ozone increase was only about 0.4% when their new rate constants for the vibrational relaxation rate for  $O_2(v)$  were used in the model calculations.<sup>110,131</sup>

## 4.2. $O_2(A^1\Delta_g)$ and $O_2(b^1\Sigma_g^+)$ Detection from the Photolysis of Ozone

The metastable  $a^1\Delta_g$  electronic state of molecular oxygen is of major importance in the emissions in the atmospheres of Earth, Venus, and Mars. One of the most intense features in the airglows of all three planets is the “infrared atmospheric band” at  $\lambda = 1.27$   $\mu\text{m}$  resulting from the (0, 0) band of the optical transition  $O_2(a^1\Delta_g \rightarrow X^3\Sigma_g^-)$ . The major source of terrestrial atmospheric  $O_2(a^1\Delta_g)$  is the daytime photolysis of ozone in the Hartley and Huggins bands. Hancock and co-workers<sup>25,61,72,132</sup> directly observed  $O_2(a^1\Delta_g)$  molecules in the photolysis of ozone between 270 and 329 nm using (2+1) REMPI via the  $O_2(3s\sigma^1\Pi_g v' = 1)$  Rydberg state with around 331.5 nm laser radiation. From the analysis of the spectral line shapes of the  $O_2(a^1\Delta_g)$  fragments in the time-of-flight spectra, they concluded that the formation of  $O_2(a^1\Delta_g)$  molecules at short wavelengths resulted mainly from the spin-allowed dissociation process



while the formation at longer wavelengths is due to the spin-forbidden dissociation processes via a curve crossing to a dissociative triplet state after the photoexcitation



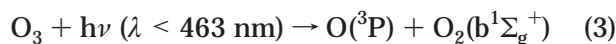
They estimate the quantum yield of the spin-forbidden process (eq 4) to be about 10% at the wavelength longer than 320 nm.<sup>61</sup> It is interesting that the two spin-forbidden photodissociation processes,  $O(^3P) + O_2(a^1\Delta_g)$  and  $O(^1D) + O_2(X^3\Sigma_g^-)$ , have almost the same quantum yield values around 8–10% from the photolysis of ozone in the UV wavelength region longer than 320 nm.

Valentini and co-workers<sup>133,134</sup> detected  $O_2(a^1\Delta_g)$  molecules in the photolysis of ozone at 17 wavelengths between 230 and 311 nm using coherent anti-Stokes Raman scattering (CARS) spectroscopy. They observed an anomalous propensity for even ( $J = 2, 4, 6, \dots$ ) rotational states in the  $O_2(a^1\Delta_g)$  fragments. They indirectly determined the quantum yield of  $0.89 \pm 0.03$  for the  $O(^1D)$  formation over the wavelength region 266–311 nm from the analysis of the odd- $J$  and even- $J$  rotational populations in the  $O_2(a^1\Delta_g)$  fragments, taking account that the curve crossing to the surface correlating to the  $O(^3P) + O_2(X^3\Sigma_g^-)$  product causes the depletion of the odd- $J$  states (see Figure 7).

Large extents of mass-independent isotope enrichment ( $^{17}\text{O}$  and  $^{18}\text{O}$ ) of ozone in the stratosphere have been observed<sup>135–138</sup> Valentini et al.<sup>134</sup> observed that in the photodissociation of  $^{48}\text{O}_3$  in the UV region the rotational population in the even  $J$  levels of the  $O_2$ -

( $a^1\Delta_g$ ) product is greater than that in the odd  $J$  levels, as described above. Using ozone enriched in  $^{18}\text{O}$ , they showed that this is not the case for  $^{18}\text{O}^{16}\text{O}$  and by inference for  $^{17}\text{O}^{16}\text{O}$ . Valentini<sup>139</sup> explained that the isotope selection comes from the curve crossing to the surface correlating to the  $\text{O}(^3\text{P}) + \text{O}_2(\text{X}^3\Sigma_g^-)$  from the surface correlated to  $\text{O}(^3\text{P}) + \text{O}_2(a^1\Delta_g)$  and that this selection in the crossing introduces a mass-independent fractionation in the photolysis, increasing the heavy isotope abundance in the product oxygen. Houston and co-workers<sup>140</sup> proposed the formation of ozone from the reaction of vibrationally excited  $\text{O}_2(v)$  with  $\text{O}_2$  as described in section 4.1. They indicated that this new source tends to distill heavy oxygen atoms into the  $\text{O}_3$  pool while depleting them from the  $\text{O}_2$  pool in the atmosphere, since the UV ozone photodissociation, which begins this ozone formation scheme, is more probable for heavy ozone than for  $^{48}\text{O}_3$ . However, recent studies have presented clear evidence that the ozone isotope enrichment in the stratosphere is attributed to the differences in the isotopic rate coefficients for the  $\text{O}_3$  formation reaction,  $\text{O} + \text{O}_2 \rightarrow \text{O}_3$ .<sup>138,141,142</sup>

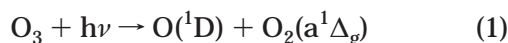
O'Keeffe et al.<sup>143,144</sup> directly observed the formation of  $\text{O}_2(b^1\Sigma_g^+)$  molecules in the photolysis of ozone at wavelengths of 340 and 351 nm using (2+1) REMPI via the  $\text{O}_2(d3s\sigma_g^1\Pi_g v' = 2)$  Rydberg state with around 351 nm laser radiation. They indicated that the  $\text{O}_2(b^1\Sigma_g^+)$  state was formed by the third spin-forbidden process in the photolysis of ozone in the Huggins band



O'Keeffe et al.<sup>143,144</sup> also measured the velocity profile of  $\text{O}(^3\text{P}_{j=0})$  produced by ozone photolysis at 322.64 nm using (2+1) REMPI detection of  $\text{O}(^3\text{P}_{j=0})$  at 226.2 nm with a time-of-flight technique. The velocity profiles indicate that the  $\text{O}(^3\text{P}_{j=0})$  fragments are produced in coincidence with  $\text{O}_2(\text{X}^3\Sigma_g^-)$ ,  $\text{O}_2(a^1\Delta_g)$ , and  $\text{O}_2(b^1\Sigma_g^+)$ . At the photolysis wavelength of 322.64 nm, the relative contributions of  $\text{O}(^3\text{P}_{j=0}) + \text{O}_2(\text{X}^3\Sigma_g^-)$ ,  $\text{O}(^3\text{P}_{j=0}) + \text{O}_2(a^1\Delta_g)$ , and  $\text{O}(^3\text{P}_{j=0}) + \text{O}_2(b^1\Sigma_g^+)$  processes were 31%, 35%, and 34%, respectively, for the  $\text{O}(^3\text{P}_{j=0})$  formation. Turnipseed et al.<sup>93</sup> estimated the formation yield of  $\text{O}_2(b^1\Sigma_g^+)$  to be  $0.50 \pm 0.38$  in the photolysis of ozone at 193 nm from the analysis of the time profile of the  $\text{O}(^3\text{P})$  resonance fluorescence. The formation of  $\text{O}_2(b^1\Sigma_g^+)$  in the photolysis of ozone in the Hartley band wavelength region has not been studied.

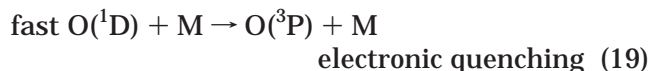
### 4.3. Nonlocal Thermal Equilibrium (non-LTE) Translational Distribution Produced by UV Photolysis of Ozone

In the stratosphere,  $\text{O}(^1\text{D})$  atoms are produced by UV photolysis of  $\text{O}_3$  in its Hartley band



where the thermochemical threshold wavelength is 309.44 nm.<sup>98</sup> When ozone molecules are photolyzed at wavelengths shorter than the threshold, the  $\text{O}(^1\text{D})$  atom formed has translational energy because of the

partitioning of the excess energy. For example, when  $\text{O}_3$  is photodissociated at 250 nm which is the maximum photoabsorption wavelength of  $\text{O}_3$  in the Hartley band, the excess energy is  $92 \text{ kJ mol}^{-1}$  and the average translational energy of the  $\text{O}(^1\text{D})$  atoms in the space-fixed frame is  $54 \text{ kJ mol}^{-1}$ .<sup>24</sup> Most of the  $\text{O}(^1\text{D})$  atoms produced in the photolysis of  $\text{O}_3$  collide with ambient air molecules ( $\text{M} = \text{N}_2, \text{O}_2$ ), and the chemical reactions of  $\text{O}(^1\text{D})$  with other minor constituents are not major rate processes of  $\text{O}(^1\text{D})$  in the atmosphere. In the stratosphere, the translationally hot (fast)  $\text{O}(^1\text{D})$  atoms are dominantly removed by translational relaxation (eq 18) or electronic quenching (eq 19) by collisions with the ambient air

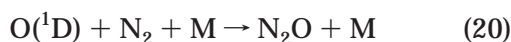


It has been believed that the translational relaxation process is fast and that the  $\text{O}(^1\text{D})$  atoms are thermally relaxed before chemical reactions. However, if the translational relaxation process (eq 18) is not so fast compared with the electronic quenching process (eq 19), the steady-state translational distribution of  $\text{O}(^1\text{D})$  deviates from the Maxwell–Boltzmann distribution at the local temperature.<sup>145–148</sup> Takahashi et al.<sup>149</sup> determined the relaxation rate of the translational energy by observing the Doppler profiles and measured the concentration change after the translationally hot  $\text{O}(^1\text{D})$  atoms were produced by the photodissociation of ozone by a KrF excimer laser at 248 nm using a vacuum UV laser-induced fluorescence detection of  $\text{O}(^1\text{D})$  at 115 nm. They indicated the competitive processes of the translational relaxation (eq 18) and the electronic quenching (eq 19) when the hot  $\text{O}(^1\text{D})$  atoms are produced by the photolysis of  $\text{O}_3$  at 248 nm experimentally, and they simulated the steady-state translational energy distributions of  $\text{O}(^1\text{D})$  in the stratosphere at the altitudes of 20–50 km. Their simulation results indicate the steady-state translational distributions of  $\text{O}(^1\text{D})$  in the stratosphere are more populated at high energies than the Maxwell–Boltzmann distributions characterized by the local ambient temperatures and that the average translational energy of  $\text{O}(^1\text{D})$ , that is, nonlocal thermodynamic equilibrium (non-LTE) conditions. At the altitude of 50 km, the average translational energy of  $\text{O}(^1\text{D})$  is about twice as large as that under thermodynamic equilibrium conditions. It is possible that the product channel branchings in the  $\text{O}(^1\text{D})$  reactions change depending on the collision energies. For instance, Brownsword et al.<sup>150</sup> reported the channel branching to form H atom in the reaction of  $\text{O}(^1\text{D})$  with  $\text{CH}_4$  at higher collision energies is larger than that at lower collision energies. In the reaction of  $\text{O}(^1\text{D}) + \text{N}_2\text{O}$ , which is the important source of  $\text{NO}_x$  in the stratosphere, the product branching between  $2\text{NO}$  and  $\text{N}_2 + \text{O}_2$  may depend on the collision energies.<sup>10,151,152</sup> Furthermore, the apparent rates of  $\text{O}(^1\text{D})$  reactions are enhanced by the non-LTE translational energy distribution, since the collision frequency becomes larger than that

under local thermodynamic equilibrium conditions. Mlynczak and Solomon<sup>153</sup> discussed the heating energy balance in the mesosphere including the hot O and O<sub>2</sub> species produced by the photodissociation of ozone.

#### 4.4. N<sub>2</sub>O Formation Associated with UV Photodissociation of Ozone

Nitrous oxide (N<sub>2</sub>O) is an important greenhouse gas. The formation of N<sub>2</sub>O by atmospheric chemical reactions has been considered. Those processes may account for a significant fraction of the oxygen mass-independent enrichment observed in atmospheric N<sub>2</sub>O and explain the altitude dependence of the observed mass-independent isotopic signature.<sup>137,154</sup> The following reaction has been considered for the formation of N<sub>2</sub>O following the production of O(<sup>1</sup>D) in the UV photolysis of ozone in the atmosphere



Collisions with the third body are required to deactivate the nascent N<sub>2</sub>O, otherwise rapid dissociation of N<sub>2</sub>O occurs. Kajimoto and Cvetanović<sup>155</sup> studied reaction 20 using a medium-pressure Hg lamp to irradiate O<sub>3</sub>/O<sub>2</sub> mixtures in 25 and 115 bar of N<sub>2</sub> diluent for 13–48 h. The N<sub>2</sub>O product was trapped cryogenically and measured using gas chromatography. Kajimoto and Cvetanović<sup>155</sup> reported a value of  $3 \times 10^{-7}$  for the quantum yield of the formation of N<sub>2</sub>O at 1 atm pressure by extrapolating the results obtained at higher pressures. Maric and Burrows<sup>156</sup> measured the three body rate constant of reaction 20 to be  $(8.8 \pm 3.3) \times 10^{-37} \text{ cm}^6 \text{ molecule}^{-2} \text{ s}^{-1}$  by irradiating a gas mixture of 0.3% O<sub>3</sub> in 1 bar synthetic air using a low-pressure Hg lamp and analyzing the N<sub>2</sub>O using a gas chromatograph. Their value is 2.5 times faster than the value derived by Kajimoto and Cvetanović.<sup>155</sup> Estupiñán et al.<sup>157</sup> measured the formation of N<sub>2</sub>O by tunable diode laser absorption spectroscopy following laser flash photolysis of O<sub>3</sub>/N<sub>2</sub>/O<sub>2</sub> gas mixtures at 266 nm. They attributed the source of N<sub>2</sub>O to reaction 20 and derived a rate constant of  $k_{20} = (2.8 \pm 0.1) \times 10^{-36} \text{ cm}^6 \text{ molecule}^{-2} \text{ s}^{-1}$  at 300 K. Using atmospheric model calculations, Estupiñán et al.<sup>157</sup> suggested that gas-phase processes initiated by ozone photolysis contribute about 1.4% of the currently estimated global source strength of atmospheric N<sub>2</sub>O. Prasad<sup>158</sup> proposed a new model in which reaction between electronically excited O<sub>3</sub> molecules and N<sub>2</sub> and also the UV photolysis of O<sub>3</sub>·N<sub>2</sub> complex contribute to N<sub>2</sub>O formation in the atmosphere.

#### 5. Conclusions

We reviewed the studies on the photodissociation processes in the ultraviolet photolysis of ozone. The formation of O(<sup>1</sup>D) atoms from ozone photolysis is one of the most important chemical processes in atmospheric chemistry, since it is followed by the generation of OH radicals and NO molecules. Recent progress on experimental techniques have made it possible to measure accurate O(<sup>1</sup>D) quantum yields

in the ozone photolysis at various temperatures and wavelengths. The thermodynamic threshold for O(<sup>1</sup>D) + O<sub>2</sub>(a<sup>1</sup>Δ<sub>g</sub>) formation is 310 nm for vibrationally cold ozone. O(<sup>1</sup>D) formation following ozone photolysis at wavelengths greater than 310 nm is attributed to absorption by vibrationally excited ozone and photodissociation through the spin-forbidden process to give O(<sup>1</sup>D) + O<sub>2</sub>(X<sup>3</sup>Σ<sub>g</sub><sup>+</sup>); a numerical expression describing the O(<sup>1</sup>D) quantum yield as functions of temperature and wavelength has been proposed based on the results of recent experimental studies.

When O<sub>3</sub> is dissociated by an UV photon, vibrationally excited O<sub>2</sub>(v) is formed. The subsequent reactions of O<sub>2</sub>(v ≥ 26) + O<sub>2</sub> were considered to produce O<sub>3</sub> in the stratosphere. However, the recent calculations based on an atmospheric models, quantum chemistry, and reaction dynamics have denied the possibility of this process. The direct experimental proof is required for the formation of O<sub>3</sub> through this process. When O<sub>2</sub> and O are separated from O<sub>3</sub> in the photodissociation, translationally hot atoms are produced due to conservation of momentum between the two photofragments. The chemical reactivity of O(<sup>1</sup>D) is so high that O(<sup>1</sup>D) in the stratosphere is not completely thermalized before it reacts. This nonthermalized atom has an average kinetic energy 2 times larger than the thermalized ones at 50 km altitude.

The atmospheric roles of the electronically, vibrationally, and/or translationally excited species which are produced by the UV photodissociation of ozone have been presented. We expect that the proposed vibrationally and translationally mediated mechanism will make a considerable contribution as new reaction mechanisms in the atmosphere. These findings are strongly related to the dynamical studies in the field of chemical physics. By applying chemical physics techniques to ozone dissociation, not only have atmospheric problems been revealed but more details about the nature of the photodissociation process have been provided.<sup>159</sup> The cooperation between basic chemical physics and atmospheric chemistry will continue to provide new findings on important processes in atmospheric chemistry.

#### 6. Acknowledgments

This work was supported by a Grant-in-Aid from the Ministry of Education, Culture, Sports, Science and Technology, Japan. We give thanks to the other members of the evaluation panel for the O(<sup>1</sup>D) quantum yields in the photolysis of ozone (Joint activity of SPARC and IGAC) for their helpful discussions and encouragement: Franz J. Comes, Gus Hancock, Andreas Hofzumahaus, Anthony J. Hynes, and A. R. Ravishankara. We are also grateful to Timothy J. Wallington and Richard Bersohn for their helpful discussions.

#### 7. References

- (1) Malicet, J.; Daumont, D.; Charbonnier, J.; Parisse, C.; Chakir, A.; Brion, J. *J. Atmos. Chem.* **1995**, *21*, 263.
- (2) Okabe, H. *Photochemistry of Small Molecules*; Wiley: New York, 1978.

- (3) Kylling, A.; Stamnes, K.; Tsay, S.-C. *J. Atmos. Chem.* **1995**, *21*, 115.
- (4) Schiff, H. I. *Ann. Geophys.* **1972**, *28*, 67.
- (5) Wayne, R. P. *Atmos. Environ.* **1987**, *21*, 1683.
- (6) Steinfeld, J. I.; Adler-Golden, S. M.; Gallagher, J. W. *J. Phys. Chem. Ref. Data* **1987**, *16*, 911.
- (7) Atkinson, R.; Baulch, D. L.; Cox, R. A.; Hampson, R. F., Jr.; Kerr, J. A.; Rossi, M. J.; Troe, J. *J. Phys. Chem. Ref. Data*, **1997**, *26*, 1329.
- (8) Atkinson, R.; Baulch, D. L.; Cox, R. A.; Hampson, R. F., Jr.; Kerr, J. A.; Rossi, M. J.; Troe, J. *IUPAC Subcommittee on Gas Kinetic Data Evaluation For Atmospheric Chemistry—Data Sheet POx2, 2001*, Website: <http://iupac-kinetic.ch.cam.ac.uk/>.
- (9) DeMore, W. B.; Sander, S. P.; Howard, C. J.; Ravishankara, A. R.; Golden, D. M.; Kolb, C. E.; Hampson, R. F.; Kurylo, M. J.; Molina, M. J. *Chemical kinetics and photochemical data for use in stratospheric modeling*; JPL Publication 94-26; JPL: Pasadena, CA, 1994.
- (10) DeMore, W. B.; Sander, S. P.; Golden, D. M.; Hampson, R. F.; Kurylo, M. J.; Howard, C. J.; Ravishankara, A. R.; Kolb, C. E.; Molina, M. J. *Chemical Kinetics and Photochemical Data for use in Stratospheric Modelling*; JPL Publication 97-4; JPL: Pasadena, CA, 1997.
- (11) Sander, S. P.; Friedl, R. R.; DeMore, W. B.; Golden, D. M.; Kurylo, M. J.; Hampson, R. F.; Huie, R. E.; Moortgat, G. K.; Ravishankara, A. R.; Kolb, C. E.; Molina, M. J. *Chemical Kinetics and Photochemical Data for Stratospheric Modeling*; JPL Publication 00-3; JPL: Pasadena, CA, 2000.
- (12) Sander, S. P.; Friedl, R. R.; Golden, D. M.; Kurylo, M. J.; Huie, R. E.; Orkin, V. L.; Moortgat, G. K.; Ravishankara, A. R.; Kolb, C. E.; Molina, M. J.; Finlayson-Pitts, B. J. *Chemical Kinetics and Photochemical Data for the Use in Atmospheric Studies, Evaluation Number 14*; JPL Publication 02-25; JPL: Pasadena, CA, 2003. Website: <http://jpldataeval.jpl.nasa.gov/>.
- (13) WMO. *Scientific assessment of ozone depletion: 1998*; Report No. 44; World Meteorological Organization: Geneva, 1999.
- (14) Brion, J.; Chakir, A.; Daumont, D.; Malicet, J.; Parisse, C. *Chem. Phys. Lett.* **1993**, *213*, 610.
- (15) Barnes, J. Mauersberger, K. *J. Geophys. Res.* **1987**, *92*, 14861.
- (16) WMO. *Atmospheric Ozone, 1985, Global Ozone Research and Monitoring Project; Report 16*; World Meteorological Organization: Geneva, 1986.
- (17) Yoshino, K.; Esmond, J. R.; Freeman, D. E.; Parkinson, W. H. *J. Geophys. Res.* **1993**, *98*, 5205.
- (18) Molina, L. T.; Molina, M. J. *J. Geophys. Res.* **1986**, *91*, 14501.
- (19) Voigt, S.; Orphal, J.; Bogumil, K.; Burrows, J. P. *J. Photochem. Photobiol., A* **2001**, *143*, 1.
- (20) Orphal, J. *J. Photochem. Photobiol., A* **2003**, *157*, 185.
- (21) Hay, P. J.; Dunning, T. H., Jr. *J. Chem. Phys.* **1977**, *67*, 2290.
- (22) Fairchild, C. E.; Stone, E. J.; Lawrence, G. M. *J. Chem. Phys.* **1978**, *69*, 3632.
- (23) Suits, A. G.; Miller, R. L.; Bontuyan, L. S.; Houston, P. L. *J. Chem. Soc., Faraday Trans.* **1993**, *89*, 1443.
- (24) Thelen, M. A.; Gejo, T.; Harrison, J. A.; Huber, J. R. *J. Chem. Phys.* **1995**, *103*, 7946.
- (25) Ball, S. M.; Hancock, G.; Pinot de Moira, J. C.; Sandowski, C. M.; Winterbottom, F. *Chem. Phys. Lett.* **1995**, *245*, 1.
- (26) Blunt, D. A.; Suits, A. G. *Am. Chem. Soc. Symp. Ser.* **1997**, *678*, 99.
- (27) Takahashi, K.; Taniguchi, N.; Matsumi, Y.; Kawasaki, M. *Chem. Phys.* **1998**, *231*, 171.
- (28) Dylewski, S. M.; Geiser, J. D.; Houston, P. L. *J. Chem. Phys.* **2001**, *115*, 7460.
- (29) Joens, J. A. *J. Chem. Phys.* **1994**, *100*, 3407.
- (30) Parisse, C.; Brion, J.; Malicet, J. *Chem. Phys. Lett.* **1996**, *248*, 31.
- (31) O'Keefe, P.; Ridley, T.; Lawley, K. P.; Donovan, R. J. *J. Chem. Phys.* **2001**, *115*, 9311.
- (32) Freeman, D. E.; Yoshino, K.; Esmond, J. R.; Parkinson, W. H. *Planet. Space Sci.* **1984**, *32*, 239.
- (33) Johnson, B. R.; Kinsey, J. L. *Phys. Rev. Lett.* **1989**, *62*, 1607.
- (34) Johnson, B. R.; Kinsey, J. L. *J. Chem. Phys.* **1989**, *91*, 7638.
- (35) Farantos, S. C.; Taylor, H. S. *J. Chem. Phys.* **1991**, *94*, 4887.
- (36) Le Quéré, F.; Leforestier, C. *J. Chem. Phys.* **1990**, *92*, 247.
- (37) Le Quéré, F.; Leforestier, C. *J. Chem. Phys.* **1991**, *94*, 1118.
- (38) Balakrishnan, N.; Billing, G. D. *J. Chem. Phys.* **1994**, *101*, 2968.
- (39) Yamashita, K.; Morokuma, K.; Le Quéré, F.; Leforestier, C. *Chem. Phys. Lett.* **1992**, *191*, 515.
- (40) Qu, Z.-W.; Zhu, H.; Schinke, R. *Chem. Phys. Lett.* **2003**, *377*, 359.
- (41) Johnson, B. R.; Kittrell, C.; Kelly, P. B.; Kinsey, J. L. *J. Phys. Chem.* **1996**, *100*, 7743.
- (42) Barinovs, G.; Markovic, N.; Nyman, G. *Chem. Phys. Lett.* **1999**, *315*, 282.
- (43) Johnson, B. R.; Chang, B.-Y.; Hsiao, C.-W.; Le, L.; Kinsey, J. L. *J. Chem. Phys.* **1998**, *108*, 7670.
- (44) Parlant, G. *J. Chem. Phys.* **2000**, *112*, 6956.
- (45) Alacid, M.; Leforestier, C. *J. Chem. Phys.* **2001**, *114*, 1685.
- (46) Lin, S. Y.; Han, K. L.; He, G. Z. *J. Chem. Phys.* **2001**, *114*, 10651.
- (47) Brand, J. C. D.; Cross, K. J.; Hoy, A. R. *Can. J. Phys.* **1978**, *56*, 327.
- (48) Katayama, D. H. *J. Chem. Phys.* **1979**, *71*, 815.
- (49) Katayama, D. H. *J. Chem. Phys.* **1986**, *85*, 6809.
- (50) Sinha, A.; Imre, D.; Goble, J. H., Jr.; Kinsey, J. L. *J. Chem. Phys.* **1986**, *84*, 6108.
- (51) Le Quéré, F.; Leforestier, C. *Chem. Phys. Lett.* **1992**, *189*, 537.
- (52) Banichevich, A.; Peyerimhoff, S. D. *Chem. Phys.* **1993**, *174*, 93.
- (53) Joens, J. A. *J. Chem. Phys.* **1994**, *101*, 5431.
- (54) Bludsky, O.; Jensen, P. *Mol. Phys.* **1997**, *91*, 653.
- (55) Sheppard, M. G.; Walker, R. B. *J. Chem. Phys.* **1983**, *78*, 7191.
- (56) Leforestier, C.; Le Quéré, F.; Yamashita, K.; Morokuma, K. *J. Chem. Phys.* **1994**, *101*, 3806.
- (57) Banichevich, A.; Peyerimhoff, S. D.; Grein, F. *Chem. Phys.* **1993**, *178*, 155.
- (58) Takahashi, K.; Kishigami, M.; Taniguchi, N.; Matsumi, Y.; Kawasaki, M. *J. Chem. Phys.* **1997**, *106*, 6390.
- (59) Zare, R. N.; Herschbach, D. R. *Proc. IEEE* **1963**, *51*, 173.
- (60) Denzer, W.; Hancock, G.; Pinot de Moira, J. C.; Tyley, P. L. *Chem. Phys. Lett.* **1997**, *280*, 496.
- (61) Denzer, W.; Hancock, G.; Pinot de Moira, J. C.; Tyley, P. L. *Chem. Phys.* **1998**, *231*, 109.
- (62) Hofzumahaus, A.; Kraus, A.; Müller, M. *Appl. Opt.* **1999**, *38*, 4443.
- (63) Lin, C. L.; DeMore, W. B. *J. Photochem.* **1973/74**, *2*, 161.
- (64) Moortgat, G. K.; Kudzus, E.; Warneck, P. *J. Chem. Soc., Faraday Trans. 2*, **1977**, *73*, 1216.
- (65) Moortgat, G. K.; Kudzus, E. *Geophys. Res. Lett.* **1978**, *5*, 191.
- (66) Philen, D. L.; Watson, R. T.; Davis, D. D. *J. Chem. Phys.* **1977**, *67*, 3316.
- (67) Arnold, I.; Comes, F. J.; Moortgat, G. K. *Chem. Phys.* **1977**, *24*, 211.
- (68) Moortgat, G. K.; Warneck, P. *Z. Naturforsch.* **1975**, *30a*, 835.
- (69) Brock, J. C.; Watson, R. T. *Chem. Phys.* **1980**, *46*, 477.
- (70) Trolter, M.; Wiesenfeld, J. R. *J. Geophys. Res.* **1988**, *93*, 7119.
- (71) Adler-Golden, S. M.; Schweitzer, E. L.; Steinfeld, J. I. *J. Chem. Phys.* **1982**, *76*, 2201.
- (72) Ball, S. M.; Hancock, G.; Murphy, I. J.; Rayner, S. P. *Geophys. Res. Lett.* **1993**, *20*, 2063.
- (73) Michelsen, H. A.; Salawitch, R. J.; Wennberg, P. O.; Anderson, J. G. *Geophys. Res. Lett.* **1994**, *21*, 2227.
- (74) Müller, M.; Kraus, A.; Hofzumahaus, A. *Geophys. Res. Lett.* **1995**, *22*, 679.
- (75) Shetter, R. E.; Cantrell, C. A.; Lantz, K. O.; Flocke, S. J.; Orlando, J. J.; Tyndall, G. S.; Gilpin, T. M.; Fischer, C. A.; Madronich, S.; Calvert, J. G. *J. Geophys. Res.* **1996**, *101*, 14631.
- (76) Armerding, W.; Comes, F. J.; Schülke, B. *J. Phys. Chem.* **1995**, *99*, 3137.
- (77) Takahashi, K.; Matsumi, Y.; Kawasaki, M. *J. Phys. Chem.* **1996**, *100*, 4084.
- (78) Takahashi, K.; Taniguchi, N.; Matsumi, Y.; Kawasaki, M.; Ashfold, M. N. R. *J. Chem. Phys.* **1998**, *108*, 7161.
- (79) Ball, S. M.; Hancock, G.; Martin, S. E.; Pinot de Moira, J. C. *Chem. Phys. Lett.* **1997**, *264*, 531.
- (80) Silvente, E.; Richter, R. C.; Zheng, M.; Saltzman, E. S.; Hynes, A. J. *Chem. Phys. Lett.* **1997**, *264*, 309.
- (81) Talukdar, R. K.; Longfellow, C. A.; Gilles, M. K.; Ravishankara, A. R. *Geophys. Res. Lett.* **1998**, *25*, 143.
- (82) Bauer, D.; D'Ottone, L.; Hynes, A. J. *Phys. Chem. Chem. Phys.* **2000**, *2*, 1421.
- (83) Smith, G. D.; Molina, L. T.; Molina, M. J. *J. Phys. Chem.* **2000**, *104*, 8916.
- (84) Hancock, G.; Tyley, P. L. *Phys. Chem. Chem. Phys.* **2001**, *3*, 4984.
- (85) Takahashi, K.; Kishigami, M.; Matsumi, Y.; Kawasaki, M.; Orr-Ewing, A. J. *J. Chem. Phys.* **1996**, *105*, 5290.
- (86) Cooper, I. A.; Neill, P. J.; Wiesenfeld, J. R. *J. Geophys. Res.* **1993**, *98*, 12795.
- (87) Kuis, S.; Simonaitis, R.; Heicklen, J. *J. Geophys. Res.* **1975**, *80*, 1328.
- (88) Fairchild, P. W.; Lee, E. K. C. *Chem. Phys. Lett.* **1978**, *60*, 36.
- (89) Talukdar, R. K.; Gilles, M. K.; Battin-Leclerc, F.; Ravishankara, A. R. *Geophys. Res. Lett.* **1997**, *24*, 1091.
- (90) Greenblatt, G. D.; Wiesenfeld, J. R. *J. Chem. Phys.* **1983**, *78*, 4924.
- (91) Amimoto, S. T.; Force, A. P.; Wiesenfeld, J. R.; Young, R. H. *J. Chem. Phys.* **1980**, *73*, 1244.
- (92) Brock, J. C.; Watson, R. T. *Chem. Phys. Lett.* **1980**, *71*, 371.
- (93) Turnipseed, A. A.; Vaghijani, G. L.; Gierczak, T.; Thompson, J. E.; Ravishankara, A. R. *J. Chem. Phys.* **1991**, *95*, 3244.
- (94) Matsumi, Y.; Comes, F. J.; Hancock, G.; Hofzumahaus, A.; Hynes, A. J.; Kawasaki, M.; Ravishankara, A. R. *J. Geophys. Res.* **2002**, *107* (D3), ACH-1, 10.1029/2001JD000510.
- (95) Taniguchi, N.; Takahashi, K.; Matsumi, Y. *J. Phys. Chem.* **2000**, *104*, 8936.
- (96) Takahashi, K.; Hayashi, S.; Matsumi, Y.; Taniguchi, N.; Hayashida, S. *J. Geophys. Res.* **2002**, *107* (D20), ACH-11, 10.1029/2001JD002048.
- (97) Stranges, D.; Yang, X.; Chesko, J. D.; Suits, A. G. *J. Chem. Phys.* **1995**, *102*, 6067.

- (98) Taniguchi, N.; Takahashi, K.; Matsumi, Y.; Dylewski, S. M.; Geiser, J. D.; Houston, P. L. *J. Chem. Phys.* **1999**, *111*, 6350.
- (99) Barbe, A.; Secroun, C.; Jouve, P. *J. Mol. Spectrosc.* **1974**, *49*, 171.
- (100) Hay, P. J.; Pack, R. T.; Walker, R. B.; Heller, E. J. *J. Phys. Chem.* **1982**, *86*, 862.
- (101) Adler-Golden, S. M. *J. Quant. Spectrosc. Radiant. Transfer* **1983**, *30*, 175.
- (102) Zittel, P. F.; Little, D. D. *J. Chem. Phys.* **1980**, *72*, 5900.
- (103) Sparks, R. K.; Carlson, L. R.; Shobatake, K.; Kowalczyk, M. L.; Lee, Y. T. *J. Chem. Phys.* **1980**, *72*, 1401.
- (104) Wine, P. H.; Ravishankara, A. R. *Chem. Phys.* **1982**, *69*, 365.
- (105) Miller, R. L.; Suits, A. G.; Houston, P. L.; Toumi, R.; Mack, J. A.; Wodtke, A. M. *Science* **1994**, *265*, 1831.
- (106) Kinugawa, T.; Sato, T.; Arikawa, T.; Matsumi, Y.; Kawasaki, M. *J. Chem. Phys.* **1990**, *93*, 3289.
- (107) Daniels, M. J.; Wiesenfeld, J. R. *J. Chem. Phys.* **1993**, *98*, 321.
- (108) Shamsuddin, S. M.; Inagaki, Y.; Matsumi, Y.; Kawasaki, M. *Can. J. Chem.* **1994**, *72*, 637.
- (109) Syage, J. A. *J. Phys. Chem.* **1995**, *99*, 16530.
- (110) Park, H.; Slinger, T. G. *J. Chem. Phys.* **1994**, *100*, 287.
- (111) Hickson, K. M.; Sharkey, P.; Smith, I. W. M.; Symonds, A. C.; Tuckett, R. P.; Ward, G. N. *J. Chem. Soc., Faraday Trans.* **1998**, *94*, 533.
- (112) Eluszkiewicz, J.; Allen, M. *J. Geophys. Res.* **1993**, *98*, 1069.
- (113) Russell, J. M., III; Gordley, L. L.; Park, J. H.; Drayson, S. R.; Hesketh, W. D.; Cicerone, R. J.; Tuck, A. F.; Frederick, J. E.; Harries, J. E.; Crutzen, P. J. *J. Geophys. Res.* **1993**, *98*, 10777.
- (114) Osterman, G. B.; Salawitch, R. J.; Sen, B.; Toon, G. C.; Stachnik, R. A.; Pickett, H. M.; Margitan, J. J.; Blavier, J.-F.; Peterson, D. B. *Geophys. Res. Lett.* **1997**, *24*, 1107.
- (115) Allen, M. *J. Geophys. Res.* **1986**, *91*, 2844.
- (116) Rogaski, C. A.; Price, J. M.; Mack, J. A.; Wodtke, A. M. *Geophys. Res. Lett.* **1993**, *20*, 2885.
- (117) Toumi, R.; Houston, P. L.; Wodtke, A. M. *J. Chem. Phys.* **1996**, *104*, 775.
- (118) Price, J. M.; Mack, J. A.; Rogaski, C. A.; Wodtke, A. M. *Chem. Phys.* **1993**, *175*, 83.
- (119) Hernández, R.; Toumi, R.; Clary, D. C. *J. Chem. Phys.* **1995**, *102*, 9544.
- (120) Balakrishnan, N.; Billing, G. D. *Chem. Phys. Lett.* **1995**, *242*, 68.
- (121) Latimer, D.; McLoughlin, P.; Wiesenfeld, J. *Geophys. Res. Lett.* **1996**, *23*, 1083.
- (122) Hernández-Lamoneda, R.; Hernández, M. I.; Carmona-Novillo, E.; Campos-Martínez, J.; Echave, J.; Clary, D. C. *Chem. Phys. Lett.* **1997**, *276*, 152.
- (123) Varandas, A. J.; Wang, W. *Chem. Phys.* **1997**, *215*, 167.
- (124) Lauvergnat, D.; Clary, D. C. *J. Chem. Phys.* **1998**, *108*, 3566.
- (125) Balakrishnan, N.; Dalgarno, A.; Billing, G. D. *Chem. Phys. Lett.* **1998**, *288*, 657.
- (126) Hernández-Lamoneda, R.; Ramírez-Solís, A. *J. Chem. Phys.* **2000**, *113*, 4139.
- (127) Jongma, R. T.; Shi, S.; Wodtke, A. M. *J. Chem. Phys.* **1999**, *111*, 2588.
- (128) Grooss, J.-U.; Müller, R.; Becker, G.; McKenna, D. S.; Crutzen, P. J. *J. Atmos. Chem.* **1999**, *34*, 171.
- (129) Slinger, T. G.; Jusinski, L. E.; Black, G.; Gadd, G. E. *Science* **1988**, *241*, 945.
- (130) Toumi, R. *J. Atmos. Chem.* **1992**, *15*, 69.
- (131) Patten, K. O., Jr.; Connell, P. S.; Kinnison, D. E.; Wuebbles, D. J.; Slinger, T. G.; Froidevaux, L. *J. Geophys. Res.* **1994**, *99*, 1211.
- (132) Ball, S. M.; Hancock, G.; Winterbottom, F. *Faraday Discuss.* **1995**, *100*, 215.
- (133) Valentini, J. J. *Chem. Phys. Lett.* **1983**, *96*, 395.
- (134) Valentini, J. J.; Gerrity, D. P.; Phillips, D. L.; Nieh, J.-C.; Tabor, K. D. *J. Chem. Phys.* **1987**, *86*, 6745.
- (135) Mauersberger, K. *Geophys. Res. Lett.* **1987**, *14*, 80.
- (136) Carli, B.; Park, J. H. *J. Geophys. Res.* **1988**, *93*, 3851.
- (137) Weston, R. E., Jr. *Chem. Rev.* **1999**, *99*, 2115.
- (138) Mauersberger, K.; Lämmerzahl, P.; Krankowsky, D. *Geophys. Res. Lett.* **2001**, *28*, 3155.
- (139) Valentini, J. J. *J. Chem. Phys.* **1987**, *86*, 6757.
- (140) Houston, P. L.; Suits, A. G.; Toumi, R. *J. Geophys. Res.* **1996**, *101*, 18829.
- (141) Janssen, C.; Guenther, J.; Krankowsky, D.; Mauersberger, K. *J. Chem. Phys.* **1999**, *111*, 7179.
- (142) Gao, Y. Q.; Marcus, R. A. *J. Chem. Phys.* **2002**, *116*, 137.
- (143) O'Keefe, P.; Ridley, T.; Wang, S.; Lawley, K. P.; Donovan, R. J. *Chem. Phys. Lett.* **1998**, *298*, 368.
- (144) O'Keefe, P.; Ridley, T.; Lawley, K. P.; Maier, R. R.; Donovan, R. J. *J. Chem. Phys.* **1999**, *110*, 10803.
- (145) Matsumi, Y.; Shamsuddin, S. M.; Sato, Y.; Kawasaki, M. *J. Chem. Phys.* **1994**, *101*, 9610.
- (146) Matsumi, Y.; Chowdhury, A. M. S. *J. Chem. Phys.* **1996**, *104*, 7036.
- (147) Balakrishnan, N.; Kharchenko, V.; Dalgarno, A. *J. Phys. Chem.* **1999**, *A103*, 3999.
- (148) Taniguchi, N.; Hirai, K.; Takahashi, K.; Matsumi, Y. *J. Phys. Chem.* **2000**, *A104*, 3894.
- (149) Takahashi, K.; Taniguchi, N.; Sato, Y.; Matsumi, Y. *J. Geophys. Res.* **2002**, *107* (D16), ACH-6, 10.1029/2001JD001270.
- (150) Brownsword, R. A.; Hillenkamp, M.; Schmiechen, P.; Volpp, H.-R.; Upadhyaya, H. P. *J. Phys. Chem.* **1998**, *A102*, 4438.
- (151) Cantrell, C. A.; Shetter, R. E.; Calvert, J. G. *J. Geophys. Res.* **1994**, *99*, 3739.
- (152) Takayanagi, T.; Akagi, H. *Chem. Phys. Lett.* **2002**, *363*, 298.
- (153) Mlynarczyk, M. G.; Solomon, S. *J. Geophys. Res.* **1993**, *98*, 10517.
- (154) Cliff, S. S.; Thiemens, M. H. *Science* **1997**, *278*, 1774.
- (155) Kajimoto, O.; Cvetanović, R. J. *J. Chem. Phys.* **1976**, *64*, 1005.
- (156) Maric, D.; Burrows, J. P. *J. Photochem. Photobiol., A: Chem.* **1992**, *66*, 291.
- (157) Estupiñán, E. G.; Nicovich, J. M.; Li, J.; Cunnold, D. M.; Wine, P. H. *J. Phys. Chem.* **2002**, *A106*, 5880.
- (158) Prasad, S. S. *J. Chem. Phys.* **2002**, *117*, 10104.
- (159) Ravishankara, A. R.; Hancock, G.; Kawasaki, M.; Matsumi, Y. *Science* **1998**, *280*, 60.

CR0205255

